Research Paper

The drift history of the Dharwar Craton and India from 2.37 Ga to 1.01 Ga with refinements for an initial Rodinia configuration

Scott R. Miller [a],*, Joseph G. Meert [a], Anthony F. Pivarunas [b], Anup K. Sinha [c], Manoj K. Pandit [d], Paul A. Mueller [a], George D. Kamenov [a]

[a] Department of Geological Sciences, University of Florida, Gainesville, FL 32601, USA
[b] U.S. Geological Survey, Geology, Minerals, Energy, and Geophysics Science Center, United States Geological Survey, Moffett Field, CA 94035, USA
[c] Dr. K.S. Krishnan Geomagnetic Research Laboratory, Chamanganj Bazaar, Allahabad 221 505, India
[d] Department of Geology, University of Rajasthan, Jaipur 302004, Rajasthan, India

A B S T R A C T

Coupled paleomagnetic and geochronologic data derived from mafic dykes provide valuable records of continental movement. To reconstruct the Proterozoic paleogeographic history of Peninsular India, we report paleomagnetic directions and U-Pb zircon ages from twenty-nine mafic dykes in the Eastern Dharwar Craton near Hyderabad. Paleomagnetic analysis yielded clusters of directional data that correspond to dyke swarms at 2.37 Ga, 2.22 Ga, 2.08 Ga, 1.89–1.86 Ga, 1.79 Ga, and a previously undated dual polarity magnetization. We report new positive baked contact tests for the 2.08 Ga swarm and the 1.89–1.86 Ga swarm(s), and a new inverse baked contact test for the 2.08 Ga swarm. Our results promote the 2.08 Ga Dharwar Craton paleomagnetic pole (43.1° N, 184.5° E; A95 = 4.3°) to a reliability score of $R = 7$ and suggest a position for the Dharwar Craton at 1.79 Ga based on a virtual geomagnetic pole (VGP) at 33.0° N, 347.5° E ($a95 = 16.9°$, $k = 221$, $N = 2$). The new VGP for the Dharwar Craton provides support for the union of the Dharwar, Singhbhum, and Bastar Cratons in the Southern India Block by at least 1.79 Ga. Combined new and published northeast-southwest moderate-steep dual polarity directions from Dharwar Craton dykes define a new paleomagnetic pole at 20.6° N, 233.1° E (A95 = 9.2°, $N = 18$; $R = 5$). Two dykes from this group yielded 1.05–1.01 Ga $^{207}Pb/^{206}Pb$ zircon ages and this range is taken as the age of the new paleomagnetic pole. A comparison of the previously published poles with our new 1.05–1.01 Ga pole shows India shifting from equatorial to higher (southerly) latitudes from 1.08 Ga to 1.01 Ga as a component of Rodinia.

© 2023 China University of Geosciences (Beijing) and Peking University. Published by Elsevier B.V. on behalf of China University of Geosciences (Beijing). This is an open access article under the CC BY-NC-ND license (http://creativecommons.org/licenses/by-nc-nd/4.0/).

1. Introduction

The Dharwar Craton of India contains a vast number of Proterozoic mafic dykes with paleomagnetic and geochronologic data that provide insight into its paleogeography (e.g., Meert et al., 2021). Although mafic dykes are attractive targets for paleomagnetic study, there are inherent difficulties when interpreting their data. For example, it is difficult to obtain datable minerals from mafic dykes and to interpret whether geochronologic results represent simultaneous dyke emplacement and magnetization (e.g., Black et al., 1991). Once an age for a dyke with paleomagnetic data is determined, that age is typically assigned to all dykes from the same craton with similar paleomagnetic directions and is referred to as a swarm. However, problems arise when different age dyke swarms yield similar directional data or paleomagnetic poles, which can occur when magnetic overprinting completely obscures primary signals (remagnetization) or from two unique magnetizations at the same location at different times (Halls, 1976, 1978; Mertanen et al., 1999; Bazhenov et al., 2016; Veselovskiy et al., 2016; Pivarunas et al., 2018). A common solution in the Dharwar Craton has been to assign ages to swarms based on dyke trends (strike), although this can also be problematic (Samal and Srivastava, 2016; Samal et al., 2019; Pivarunas and Meert, 2020; Pivarunas et al., 2021). These difficulties are common in Proterozoic paleomagnetic studies but can be resolved through identification of partial and complete magnetic overprints, the determination of characteristic magnetization carriers through rock magnetism, and geochronological analysis (Bilardello, 2019; Meert et al., 2020).

* Corresponding author.
  E-mail address: scottrimiller@ufl.edu (S.R. Miller).

This contribution focuses on two intervals of mafic magmatism in the Dharwar Craton from 2.37 Ga to 1.79 Ga and 1.14–1.01 Ga. These periods of mafic dyke and kimberlite pipe emplacement are interesting because they correlate with the formation of the Columbia and Rodinia supercontinents at ~1.8–1.6 Ga and ~1.1–1.0 Ga, respectively, and may yield insight into tectonic and magnetic phenomena during these major events in Earth's history (e.g., Meert and Torsvik, 2003; Li et al., 2008; Meert, 2012; Meert and Santosh, 2017, 2022). In recognition that dyke emplacement for individual swarms may take place over several million years (m.y.), we refer to dyke swarms by their average age in billions of years rounded to the nearest ten m.y. (e.g., 2.37 Ga). We also refer to the swarms by their ages because geographical names can be misleading.[1] High-precision (U-Pb/Pb-Pb baddeleyite, U-Pb zircon, and U-Pb perovskite) geochronological analyses for mafic–ultramafic intrusive units of the Dharwar Craton yield average swarm ages of 2.37 Ga, 2.25 Ga, 2.22 Ga, 2.21 Ga, 2.18 Ga, 2.08 Ga, 1.96 Ga, 1.89–1.88 Ga, 1.86 Ga, 1.79 Ga, 1.19 Ga, and 1.14–1.08 Ga. Each swarm is associated with paleomagnetic data except the 1.96 Ga and 1.79 Ga swarms. The swarms' geographical names, age details, and references are listed in Supplementary Data S1.

Discussing dyke swarm ages as accurate to the nearest ten m.y. rather than to the nearest single m.y. deviates from our previous approach as well as from that of other publications focused on the Precambrian mafic dyke swarms of India (e.g., Kumar et al., 2012a, 2012b, 2015; Nagaraju et al., 2018a, 2018b; Yadav et al., 2020; Meert et al., 2021; Pivarunas et al., 2021; Srivastava et al., 2021). These publications refer to dyke swarm ages in millions of years (e.g., 2367 Ma) when discussing geochronologic and paleomagnetic results, but often switch to billions of years (Ga) when correlating cratons in continental to global paleogeographic reconstructions or when discussing potential large-igneous provinces (LIPs). Although < 1 m.y. age precision of mafic dykes can be achieved with U-Pb/Pb-Pb baddeleyite geochronology, non-overlapping U-Pb baddeleyite ages are cited for the same 2.37 Ga paleomagnetically-correlated "dyke swarm" (e.g., 2369 ± 1 Ma and 2365 ± 1 Ma ages from French and Heaman (2010)). Also, average ages of dyke swarms are subject to change as new sites with paired paleomagnetic and geochronologic data are added. Estimates for shallow dyke and sill solidification indicate cooling

occurs on short timescales, e.g., days to kiloyears (k.y.), depending on dyke thickness and emplacement depth (Turcotte and Schubert, 2002). However, higher geothermal gradients in the Proterozoic, uncertainty about dyke emplacement depth, and uncertainty about the extent of magmatic plumbing systems associated with dyke swarms (including possible crystallization of zircon/baddeleyite in magma chambers in the lower-middle crust prior to magma transport and solidification) all limit our understanding of their cooling, crystallization, and magnetization histories (e.g., Halls, 1982; Huppert and Sparks, 1985; Black et al., 1991; Artemieva and Mooney, 2001; Magee et al., 2019; Buchan and Ernst, 2021). Furthermore, if we assume typical plate motion rates of ~5–10 cm/yr, then a 10-million-year time frame will encompass the error envelopes of most high quality paleomagnetic poles. For these reasons, we see the x.xx Ga age assignments for mafic dyke swarms as a useful approximation for this contribution.

1.1. The geology of India

The geology of Peninsular India is broadly characterized by five distinct Archaean terranes separated by Proterozoic and younger sedimentary basins, collectively named the Purana basins, and Proterozoic metamorphic mobile belts (Wadia, 1919; Sarkar et al., 1964; Crawford and Compston, 1973; Radhakrishna and Naqvi, 1986; Rogers, 1986; Naqvi and Rogers, 1987; Radhakrishna, 1987; Kale and Phansalkar, 1991; Chaudhuri et al., 2002; Meert et al., 2010; Meert and Pandit, 2015). The mobile belts include the Aravalli-Delhi Mobile Belt (within the broader Aravalli Region; Saha et al., 2008; Bhowmik et al., 2010, 2018; Singh et al., 2010; McKenzie et al., 2013), the Central Indian Tectonic Zone (CITZ; Yedekar, 1990; Jain et al., 1995; Eriksson et al., 2006; Bhowmik, 2019), and the Eastern Ghats Mobile Belt (Giri et al., 2022) (Fig. 1). The extensive ~ ENE-WSW trending CITZ separates the Indian cratons into the North India Block (NIB) and the South India Block (SIB). The NIB consists of the Aravalli Region, the Bundelkhand Craton, and the Marwar Block (whose age is debated but is likely > 1 Ga), while the SIB consists of the Singhbhum, Bastar, and Dharwar Cratons (Fig. 1; Mazumder et al., 2000; Acharyya, 2003; Naqvi, 2005; Sharma, 2009; Meert et al., 2010; Bhowmik et al., 2012; Davis et al., 2014; Meert and Pandit, 2015; Zhao et al., 2018b; Bhowmik, 2019; Dey et al., 2019; Ghosh et al., 2022). The *meso*- to Neoproterozoic Eastern Ghats Mobile Belt (hereafter referred to as the Eastern Ghats) marks the eastern edge of the Indian subcontinent and may represent a suture between the Rayner and Napier Complexes of East Antarctica and the Dharwar Craton (e.g., Grew and Manton, 1986; Mezger and Cosca, 1999; Sengupta et al., 1999; Fitzsimons, 2000a, 2000b, 2003; Dasgupta and Sengupta, 2003; Boger, 2011; Bose et al., 2011; Meert et al., 2017; Pandit et al., 2022). The Mesozoic Western Ghats Mobile Belt (or Western Ghats) bounds India on its western side and formed during the breakup of Gondwana (e.g., Storey, 1995; Dutta et al., 2004; Sheth et al., 2009; Chetty et al., 2012). The Dharwar Craton is divided into eastern and western domains (Eastern Dharwar Craton (EDC) and Western Dharwar Craton (WDC)) separated by the N—S trending 2.53–2.52 Ga Closepet Granite batholith (Naqvi and Rogers, 1983; Friend and Nutman, 1991; Jayananda et al., 1995, 2000, 2013, 2018; Chadwick et al., 1997, 2000; Moyen et al., 2001, 2003a, 2003b; Meert et al., 2010; Bhattacharya, 2019; Peng et al., 2019). The Dharwar Craton includes a portion of the Southern Granulite Terrane, specifically the high-grade terrane north of the Palghat Cauvery Shear Zone, and is bordered by the Western Ghats, Deccan Traps, and Arabian Sea to the west and north and the Eastern Ghats and the Pranhita-Godavari rift basin to the east (Fig. 1; Naqvi and Rogers, 1983; Dash et al., 2013; Pivarunas et al., 2019).

---

[1] Söderlund et al. (2019) named the dyke swarms of the Dharwar Craton based on cities/townships where dykes of each swarm were first dated (e.g., the 2.18 Ga Mahabubnagar swarm from Pandey et al. (1997)). However, as new studies provide new age data, it is becoming evident that many Paleoproterozoic dyke swarms are widespread throughout the craton and that geographic names are not reflective of the extent of the swarms. For example, in the Eastern Dharwar Craton (EDC), some 2.25 Ga dykes of the Ippaguda-Dhiburahalli swarm exist near Mahabubnagar, whereas 2.18 Ga dykes of the Mahabubnagar swarm and 2.08 Ga dykes of the Devarabanda swarm are found near Ippaguda (Fig. 1; Söderlund et al., 2019). 2.22–2.21 Ga dykes of the Kandlamadugu and Anantapur-Kunigal swarms have also been recently dated further northwest and southwest in the Western Dharwar Craton (WDC; Yadav et al., 2020). Fig. 1 illustrates that many swarms nearly span the latitudinal length of the craton and that the 2.18 Ga swarm nearly spans its longitudinal length. Continuing to add localities to a name is cumbersome, and while geographic names do not necessarily limit the presence of a swarm to a locality or preclude the presence of other swarms in that specific area, they may mislead unfamiliar readers into thinking the geographic name represents a central location from which the swarm emanates. For example, Yadav et al. (2020) traced the trends of the 2.22 Ga Kandlamadugu swarm, the 2.21 Ga Anatapur-Kunigal swarm, and the 2.18 Ga Mahabubnagar-Dandeli swarm of the EDC and the WDC to an intersection at the northwest edge of the WDC and hypothesized a mantle plume centered at this location. The basic assumption of Yadav et al. (2020) that these dyke swarms are radiating requires further support, and thus illustrates the current lack of constraining factors when hypothesizing a central origin for dyke swarms. Because the geographic center of Dharwar Craton dyke swarms is poorly constrained, we refrain from using geographic descriptors of each swarm and instead only use ages.
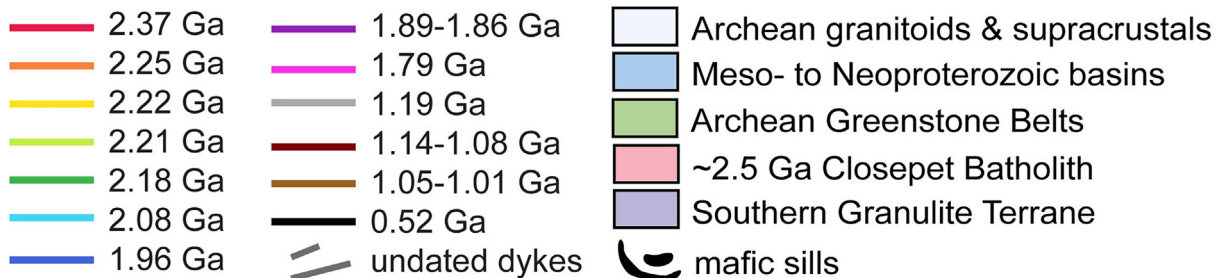
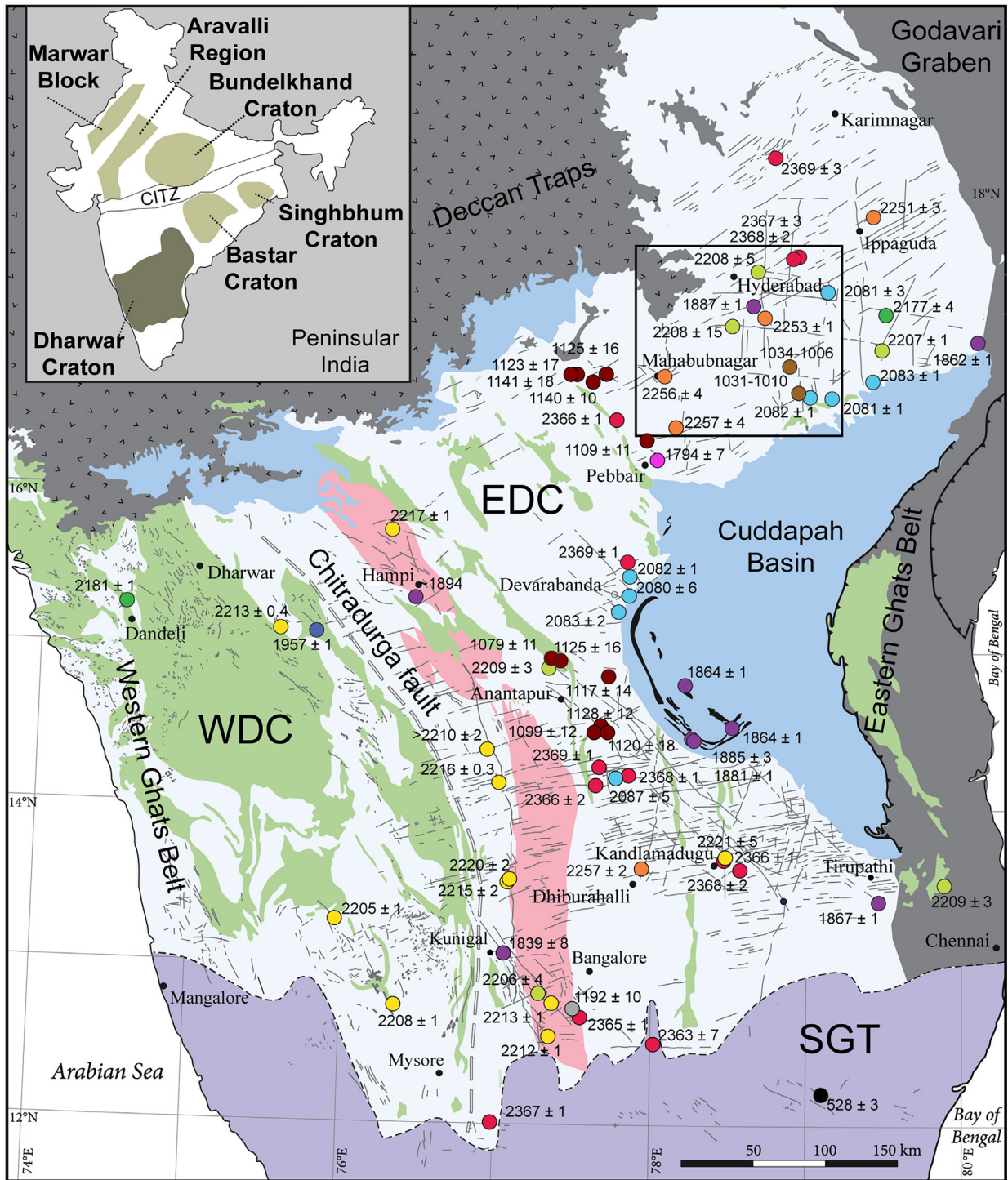**Fig. 1.** Generalized geologic map of the Dharwar Craton and study area (black box) modified from Demirer (2012). Major lithologic groupings are represented by pastel colors and U-Pb or Pb-Pb dated Proterozoic dykes are represented by colored circles. EDC: Eastern Dharwar Craton; WDC: Western Dharwar Craton. Top left inset shows the five major cratonic nuclei of Peninsular India, the Marwar Block, and the CITZ.

1.2. India's paleomagnetic record

Meert et al. (2021) summarized the paleomagnetism of Precambrian Peninsular India based on eleven high quality paleomagnetic poles from 2.37 Ga to 0.77 Ga, although early Paleoproterozoic connections between Indian cratons were considered speculative. For example, they included a single paleomagnetic direction from a 2.37 Ga Bastar Craton dyke that agrees with the 2.37 Ga Dharwar Craton directions, suggesting the possibility of a Dharwar-Bastar unification by this time (Halls et al., 2007; French and Heaman, 2010; Kumar et al., 2012a; Liao et al., 2019; Pivarunas et al., 2019; Söderlund et al., 2019; Sarma et al., 2020). 2.25 Ga dyke swarms exist in the Dharwar, Bastar, and Singhbhum Cratons, which warrants paleomagnetic tests for a 2.25 Ga SIB unification (Nagaraju et al., 2018a; Söderlund et al., 2019; Srivastava et al., 2019, 2021). Pivarunas et al. (2021) showed that a Dharwar-Singhbhum match at 2.25 Ga is possible through a rotation of Singhbhum Craton paleomagnetic poles. Paired paleomagnetic-geochronologic results for the 2.25 Ga Dharwar Craton swarm could confirm this hypothesis but are currently unavailable (see Section 5.1).

Meert et al. (2021) concluded that the SIB amalgamated by at least 1.77 Ga and that Peninsular India was united no later than 1.1–0.9 Ga, meaning that the SIB is permissible in Columbia supercontinent reconstructions, and a fully assembled Peninsular India is permissible in Rodinia. Meert et al. (2021) based their 1.77 Ga minimum age of SIB coalescence on combined evidence from the 1.89 Ga paleomagnetic pole (referred to in this contribution as the 1.89–1.86 Ga pole) shared between the Dharwar and Bastar Cratons and coeval 1.79–1.77 Ga dyke swarms in both the Dharwar and Singhbhum Cratons (ages from Halls et al., 2007; French et al., 2008; Belica et al., 2014; Shankar et al., 2014; Nagaraju et al., 2018b; Söderlund et al., 2019; Sarma et al., 2020). Pisarevsky et al. (2013) reported a 1.47–1.45 Ga paleomagnetic pole for the Lakhna dykes of the Bastar Craton, although this has yet to be correlated to the rest of the SIB.

Evidence for Peninsular India assembly during Rodinia formation comes from agreement between paleomagnetic poles of the Mahoba dykes (1.11 Ga; Pradhan et al., 2012; Radhakrishna et al., 2013a), the Majhgawan kimberlite (1.07 Ga; Miller and Hargraves, 1994; Gregory et al., 2006), and the Bhander-Rewa sedimentary rocks (~1.0 Ga; Athavale et al., 1972; Klootwijk, 1973; McElhinny et al., 1978; Malone et al., 2008) of the Bundelkhand Craton with 1.13–1.08 Ga Wajrakarur kimberlites of the Dharwar Craton (Venkateshwarlu and Chalapathi Rao, 2013; Meert et al., 2021). In addition to the paleomagnetic data, there are strong geological and geophysical arguments for ca. 1.1–0.9 Ga assembly of the NIB and SIB along the CITZ (Bhowmik et al., 2012; Mandal et al., 2013; Meert et al., 2013; Chatterjee, 2018; Bhowmik, 2019; Chattopadhyay et al., 2020). Despite these connections, refinements are still possible for the Proterozoic paleogeographic history of the Dharwar Craton, the SIB, and Peninsular India as a whole, particularly during intervals where multiple swarms and paleomagnetic poles have been reported, i.e., from 1.89 Ga to 1.86 Ga in the Dharwar Craton, and in the Mesoproterozoic where Q/R scores are low (Van der Voo, 1990; Meert et al., 2020).

2. Sampling and analysis

Paleomagnetic and geochronologic sampling of mafic dykes focused on two areas ~90 km southeast and southwest of Hyderabad, Telangana, surrounding the towns of Mahabubnagar and Devarakonda (Figs. 1 and 2). Large dykes visible on satellite imagery were often too weathered to retrieve quality (e.g., *in situ*) samples, but they served as a guide for locating smaller dykes in the vicinity. The highest quality sites were fresh dyke exposures in dry riverbeds and freshly blasted quarries. Most sites were clustered south of Devarakonda in an unnamed drainage channel that flows into the Pedda Vagu Reservoir or centered around Mahabubnagar (Fig. 2). Site 34 is distal from the two main sampling areas and is located ~45 km northeast of Hyderabad (Fig. 2). Most of the sampled dykes exhibited N-S, E-W, or ENE-WSW trends and all were vertical to subvertical, providing no evidence for post-emplacement tilting in this tectonically stable portion of the Dharwar Craton. Samples were collected and processed using standard procedures for paleomagnetic study outlined in Tauxe (2010).

Sample specimens were treated with either thermal demagnetization using an ASC TD-48 thermal demagnetizer or alternating field (AF) demagnetization using a DTech 2000 AF demagnetizer at the University of Florida. Split thermal/AF pilot demagnetization of specimens from the same sample dictated site-level demagnetization schema. A Molspin Spinner magnetometer was used to measure high intensity specimens and a 2G-77R cryogenic magnetometer was used to measure lower intensity specimens. Characteristic remanent magnetizations (ChRMs) were isolated using linear segments of paleomagnetic vector directions on Zijderveld (2013) plots or through great circle analysis (GCA; Halls, 1976, 1978) following stepwise thermal or AF demagnetization. Paleomagnetic vector directions were determined using principal component analysis (PCA) in Interactive Analysis of Paleomagnetic Data (IAPD) software from Torsvik et al. (2016) (Kirschvink, 1980). GMAP 2015 software (T.H. Torsvik) was used to convert ChRM directions and common overprints from sites into VGPs, to calculate paleomagnetic poles from VGP groups, and to create continental reconstructions. Bulk magnetic susceptibility and susceptibility vs temperature (Curie temperatures) were measured using a Kappabridge KLY-3S with CS-3 furnace attachment and hysteresis of specimens was measured using a Princeton Instruments Model 3900 vibrating sample magnetometer (VSM).

Several samples from coarse grained dykes were crushed for U-Pb dating of zircons. Zircons were separated from other < 300-μm grains by hydrodynamic/density (Gemini table and heavy liquid tetrabromoethane) and magnetic (Frantz LB-1 Magnetic Barrier Laboratory Separator) methods, and then hand-picked under a binocular microscope. Sample zircons and FC-1 Duluth Gabbro standard were mounted in epoxy resin and polished prior to backscattered-electron (BSE) and cathodoluminescence (CL) imaging with an EVO MA10 XVP scanning electron microscope. With guidance from BSE/CL images, FC-1 standard and unknown specimens were ablated using an Applied Spectra tandem 213 nm Nd-YAG laser with a 20-μm beam diameter. The ablated particles were carried in a He stream to a Nu Plasma I multi-collector inductively coupled plasma mass spectrometer (LA-MC-ICP-MS). The raw U-Pb data were reduced off-line, and ages were calculated from measured $^{207}Pb/^{206}Pb$ and $^{206}Pb/^{238}U$ ratios using decay constants from Steiger and Jäger (1977) in CALAMARI software (P.A. Mueller, University of Florida, written communication, 2020). The calculated U-Pb ages were plotted using ISOPLOTR online software (Vermeesch, 2018).

3. Paleomagnetic results

Stable paleomagnetic directions were discernable for twenty-nine sites, each from a unique dyke. This yielded five directional groupings: steep up (2 dykes), northeast shallow (7 dykes), west-northwest shallow up (12 dykes), west-northwest shallow down (2 dykes), and northeast-southwest moderate-steep dual polarity (6 dykes) (Fig. 3a). All ChRMs with inclinations steeper than − 70° are included in the steep up group and all ChRMs with inclinations between 40° and 70° (absolute value) are included in
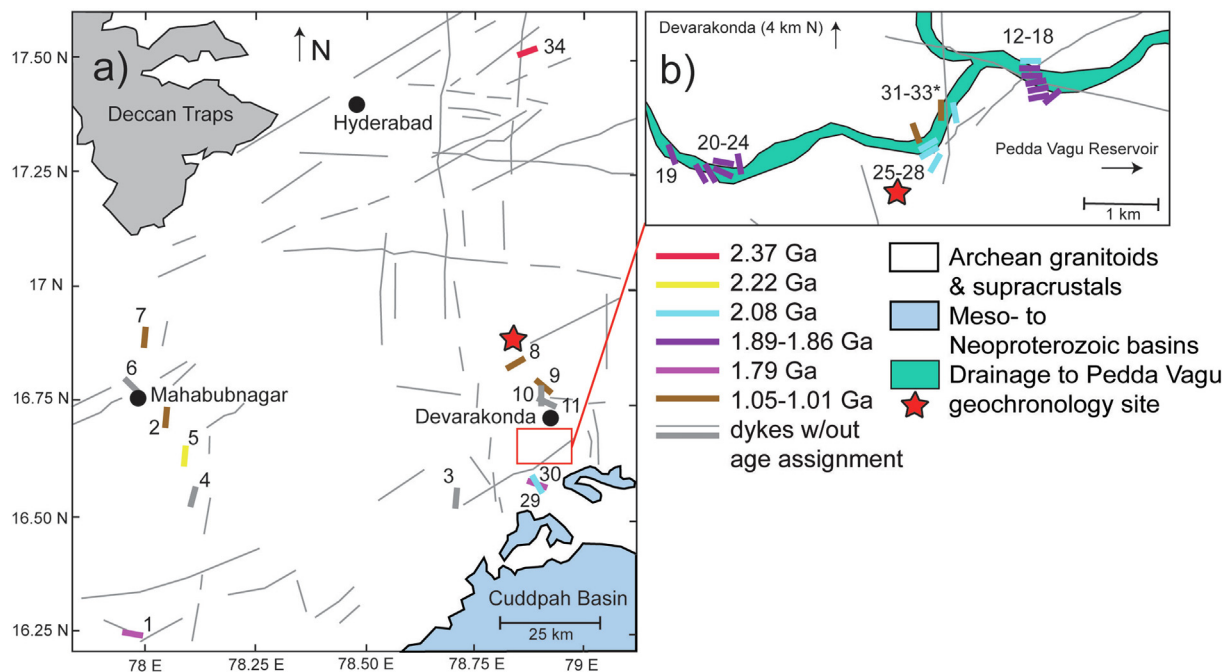
Fig. 2. The study area, including dyke site locations, trends, and their interpreted ages. (a) Zoomed out view of all dyke sites. (b) Concentrated dyke site locations south of Devarakonda. Thick gray lines indicate dykes that were sampled but did not yield consistent directions. *Indicates spider dyke with multiple trends.
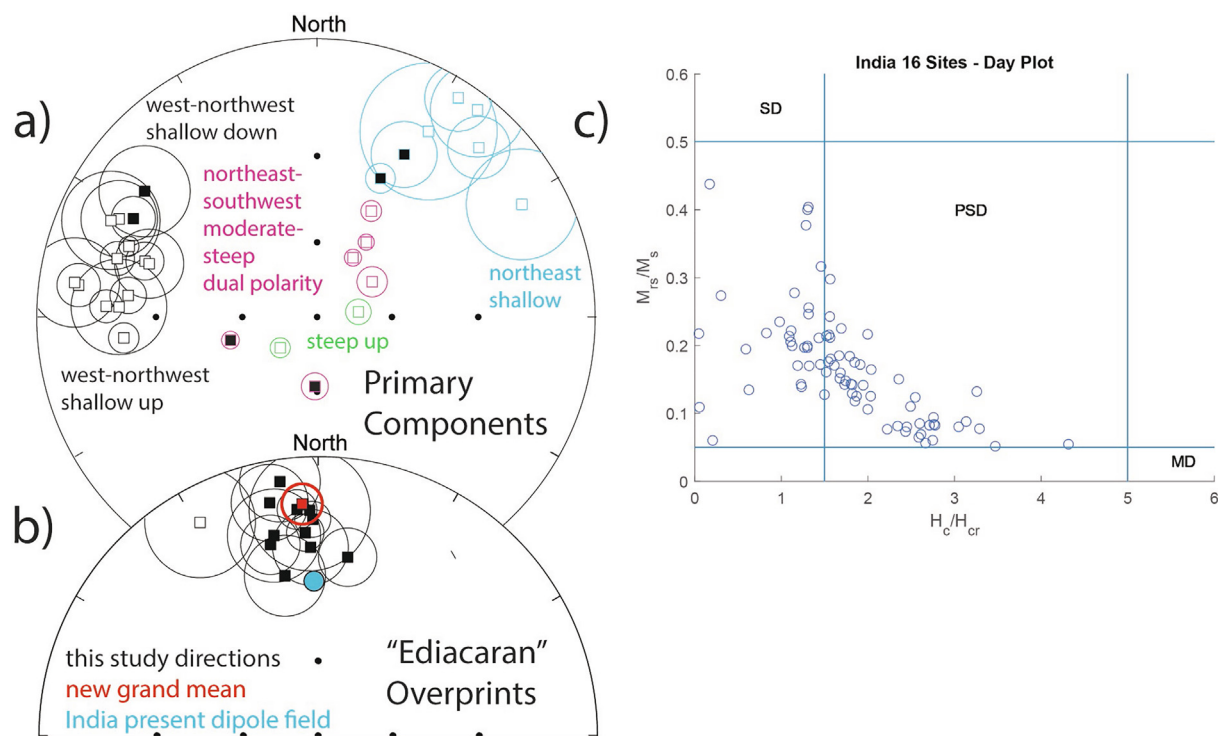

Fig. 3. Summary of demagnetization results (a, b) and rock magnetic results (c) from this study. The directional data in (a) and (b) are projected through the lower hemisphere of Wulff stereonet plots, with filled/open squares indicating down/up inclinations, and where down inclinations represent "normal" (or present-day) field. This convention is also used in representations of directional data in Figs. 4–10. (a) Site-level ChRM means color-coded by directional group. (b) Selected site-level secondary component means from this study and a new grand mean representing the "Ediacaran remagnetization" plotted along with the direction of Earth's present-day dipole field for Hyderabad at $D = 359°$ (WMM 2019–2024), $I = +32°$, calculated from dipole equation. (c) Day Plot showing bulk susceptibility data from specimens from all sites (SD: single domain; PSD: pseudo-single domain; MD: multi-domain).

the northeast-southwest moderate-steep dual polarity group. Twelve sites exhibited north shallow down overprints at low temperatures and coercivities with a mean $D = 354°$, $I = +17°$

$(a95 = 5.4°, k = 72)$ (Fig. 3b, Table 1). These overprints are consistent with the widespread "Ediacaran remagnetization" in the Southern Granulite Terrane proposed by Halls et al. (2007),

Table 1
Consistent site-level secondary components that resemble the craton-wide "Ediacaran remagnetization".

Site	Slat (°)	Slong (°)	Trend	N/n	D (°)	I (°)	a95 (°)	k (K)	Plat (°N)	Plong (°E)	A95 (°)	Refs.
2	16.6952	78.0700	0	14	355	12	4.9	67	78.2	283.1		1
5	16.5984	78.0993	10	18	359	14	4.6	58	80.7	264.2		1
7	16.8721	78.0228	5	17	356	18	5.0	51	81.3	285.2		1
13	16.6539	78.9141	90	5	348	29	12.3	40	78.4	345.8		1
14	16.6539	78.9141	90	7	346	20	8.1	57	74.9	325.0		1
16	16.6539	78.9141	80	8	351	5	8.9	40	73.2	291.6		1
20	16.6416	78.8767	170	7	331	−8	12.7	24	54.8	316.0		1
25	16.6451	78.8996	30	8	9	24	8.4	45	80.1	191.9		1
26	16.6444	78.9012	160	11	358	12	14.8	11	79.3	269.7		1
29	16.5473	78.8905	160	8	358	22	10.6	28	84.5	279.7		1
30	16.5473	78.8905	110	10	348	9	9.1	29	73.1	304.5		1
32	16.6478	78.9036	0	2	348	17	12.3	417	76.0	316.9		1
Mean				12/115	354	17	5.4	72	78.2	299.5	5.7	1
Ag-Anaik.				2/10	14	27	26.1	94	76.0	152.1	15.9	2
Dharm.				5/29	360	9	10.8	51	82.6	258.2	10.3	2
Halls 'B'				5/36	357	−3	7.3	110.6	75.9	269.9	5.3	3
Pivarunas 'B'				10/88	355	8	12.9	15	80.6	287.8	10.7	4
Grand mean^				33/276	356	10	5.3	23	80.8	280.5	4.2	1

Notes: Slat = site latitude, Slong = site longitude, Trend = trend of dyke, *N* = number of dyke sites whose data were used in the calculation of the mean direction, *n* = number of specimens analyzed from each site, *D* = declination, *I* = inclination, a95 = cone of 95% confidence about the mean direction, *k* = site-level kappa precision parameter (Fisher, 1953), K = precision parameter for meal pole, Plat = pole latitude, Plong = pole longitude, A95 = radius of the 95% confidence circle about the mean pole. Refs: 1. This Study, 2. Radhakrishna and Joseph (1996), 3. Halls et al. (2007), 4. Pivarunas et al. (2019). ^ Calculated after removal of sites with *n* < 4 and a95 > 15°. Site 20 from Pivarunas et al. (2019) was also removed from the grand mean calculation due to being outside the Vandamme cutoff = 28.9°.

Pradhan et al. (2008), and Pivarunas et al. (2019). With our additions, a new grand mean calculated for this direction in the Dharwar Craton and Southern Granulite Terrane yields a paleomagnetic pole at 80.8° N, 280.5° E (A95 = 4.2°, *N* = 33; Table 1). Despite its prevalence, the "Ediacaran remagnetization" lacks absolute age constraints and requires further investigation.

Demagnetization results and rock magnetic results verified magnetite as the dominant magnetic carrier for all sites. For example, Figs. 4–10 and Tables 2–6 show ChRM directions for the dyke groups isolated at temperatures between 500 and 580 °C or with coercivities between 30 and 50 mT, characteristic of elongated single domain magnetite in rocks (Dunlop and Özdemir, 2001). Sometimes, magnetic remanence was observed in specimens beyond these temperatures and coercivities indicative of hematite as a remanence carrier with limited influence on ChRM directions (e.g., Figs. 5c, 7c, d; Lowrie, 1990). Sharp decreases in susceptibility at 580 °C were observed in susceptibility vs temperature curves (Figs. 4, 5, 7, 9, 10). Several samples show differences in heating and cooling curves indicative of alteration of high-Ti titanomagnetite, with Curie temperatures as low as 150–200 °C at TM60, or pyrrhotite, with a Curie point from 225 to 320 °C (Dunlop and Özdemir, 2001; Li et al., 2014). Hysteresis loops show narrow shapes indicating the presence of low coercivity ferrimagnetic minerals (i.e., magnetite and maghemite) (Figs. 4, 5, 7, 9, 10). Single domain and pseudo-single domain (or vortex state) behavior was observed in most samples and is shown in the Day Plot in Fig. 3c (Day et al., 1977; Dunlop, 2002).

3.1. Steep up directions (2.37 Ga and 2.22 Ga)

Steep up ChRM directions were isolated from Sites 5 and 34 using thermal and AF demagnetization. Sharp decreases in magnetization at 580 °C in susceptibility vs temperature curves indicate magnetite as the dominant remanence carrier for both sites (Fig. 4c, d).

Overlapping temperature and coercivity spectra were observed in Zijderveld plots of demagnetization data for Site 34, so GCA was used to determine the site ChRM. The great circles intersect at *D* = 083°, *I* = − 73° (maximum angular deviation (MAD) = 5.1°), indicating a northeast steep up ChRM for the dyke (Fig. 4a, Table 2). Site 34 in this study is the NE-SW trending 2.37 Ga Bhongir dyke

from Söderlund et al. (2019) and its northeast steep up ChRM direction resembles other primary magnetizations for 2.37 Ga dykes. Although its reported location is imprecise, the 2.37 Ga Dyke-2 (or HY-67) from Kumar et al. (2012a) may also be from the Bhongir dyke and matches Site 34 with an east steep up ChRM. The resultant VGP for Site 34 is 11.3° N, 47.0° E, which falls within the swathe of 2.37 Ga VGPs in the Meert et al. (2021) Dharwar-Bastar grand mean compilation, centered at 13° N, 62° E (A95 = 4.6°).

Low temperature/coercivity overprints from Site 5 were removed by 300–550 °C or 15 mT and clustered in a north shallow down direction, resembling the Ediacaran remagnetization (Fig. 4b). Two distinct directions were obtained from Site 5 during high temperature demagnetization between 450 and 570 °C: northeast steep up high-temperature directions with a mean *D* = 038°, *I* = − 74° (a95 = 3.0°, *k* = 301, *n* = 9 specimens) were obtained from specimens 1a-4c (located close to the contact with country rock), whereas southwest steep up high-temperature directions with a mean *D* = 230°, *I* = − 71° (a95 = 4.0°, *k* = 151, *n* = 10) were obtained from specimens 5b-8e (central portion of the dyke) (Fig. 4b, Table 2). The northeast steep up component was isolated in specimen 5a (the only AF demagnetized specimen) between 15 and 60 mT. Several thermally demagnetized central dyke specimens remained in the northeast-up sector between 400 and 520 °C before an intensity increase and movement to the southwest steep up component (Fig. 4b). Bulk susceptibility is higher in the central dyke specimens (average κ of 1.7×10^{-3} vs 9.7×10^{-4} SI), which is indicative of coarser grain sizes of multi-domain magnetite. The southwest steep up component observed in thermally demagnetized specimens from the central dyke coincides with hard-shouldered intensity decay curves (Fig. 4b). We consider the southwest steep up direction as the ChRM for the dyke, yielding a VGP at 35.8° N, 110.4° E. The dyke is likely part of the 2.22 Ga swarm based on its agreement with the Meert et al. (2021) mean paleomagnetic pole at 34° N, 124° E (A95 = 6.6°).

3.2. Northeast shallow directions (2.08 Ga)

Seven dykes (Sites 12, 26, 27, 28, 29, 32, 33) exhibit northeast shallow directions (mean *D* = 037°, *I* = +02°; a95 = 16.8°, *k* = 14;
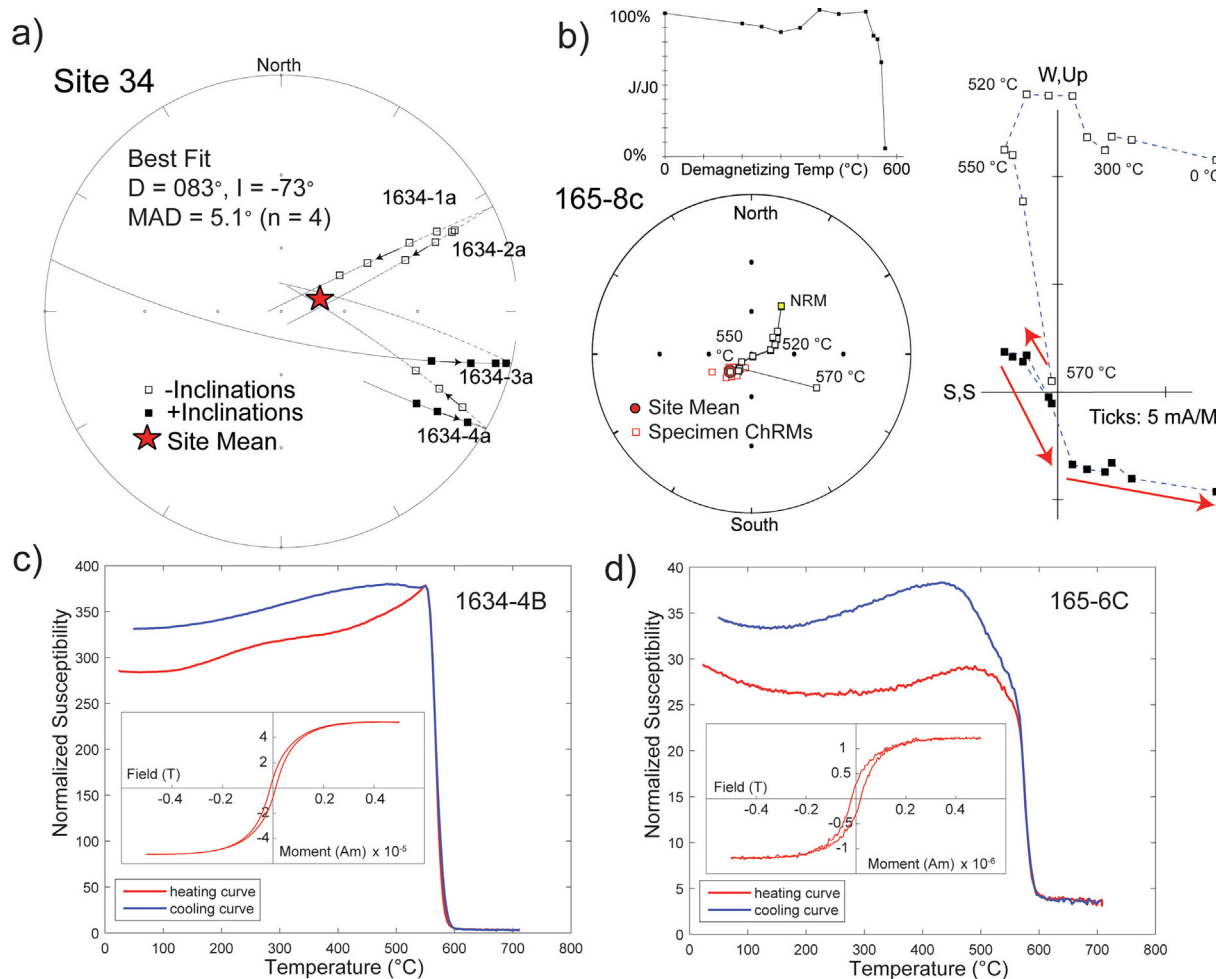
Fig. 4. Demagnetization and rock magnetic results for steep up sites, Site 34 (a,c) and Site 5 (b,d). (a) Site 34 GCA showing specimens movement towards and eventual intersection with a northeast steep up ChRM direction. (b) Zijderveld plot (PCA), intensity decay curve, and stereoplot for specimen 165-8c, along with the site mean direction. NRM = natural remanent magnetization. In (c) and in all other stereonet representations depicting stepwise demagnetization in Figs. 5–10, yellow squares indicate "up" starting points and blue squares indicate "down" starting points. (c–d) Susceptibility vs temperature curves and narrow hysteresis loops for specimens from Site 34 and Site 5. (For interpretation of the references to color in this figure legend, the reader is referred to the web version of this article.)

Fig. 5a; Table 3) isolated at temperatures from 530 to 600 °C or coercivities from 25 to 180 mT. Site 26, 29, 32, and 33 specimens exhibited north shallow down overprints removed at lower temperatures and coercivities. Susceptibility vs temperature curves exhibit sharp decreases in magnetization at 580 °C indicating magnetite as the main remanence carrier for the samples (Fig. 5b). Site 28 was demagnetized primarily with AF because the AF treatment isolated directional components more clearly than thermal methods. The AF demagnetized specimens yielded two distinct components (Fig. 5c). The first was a northeast moderate-steep up, low coercivity component with $D = 039°$, $I = -53°$ ($a95 = 4.9°$, $k = 97$, $n = 10$) that was removed between 0 and 20 mT (less often 0–70 mT) or between 125 and 500 °C prior to isolation of the northeast shallow down ChRM. Thermally demagnetized specimens from Site 28 only carried the northeast moderate-steep up component (Fig. 5d). Babu et al. (2018) also sampled the Site 12 dyke (their DK 4) reporting a secondary "B" component of $D = 035°$, $I = -39°$ ($a95 = 7°$, $k = 43$), but no other directions.

A baked contact test was performed at Site 27 (Fig. 6). The thermal/AF demagnetized Site 27 dyke specimens showed univectorial decay towards the northeast shallow down ChRM (mean $D = 025°$, $I = +33°$; $a95 = 4.7°$, $k = 167$, $n = 7$; Fig. 6a; Table 3). After removal of a north-northwest shallow-down overprint, the baked zone granites show a northeast shallow down direction that matches the dyke

ChRM (Fig. 6b). Unbaked granitoid specimens at the nearby Site 26 exhibit a nearly univectorial north-northwest shallow down magnetization (Fig. 6c). Because these north-northwest shallow down components resemble the proposed regional Ediacaran remagnetization, it is possible that the baked zone (from Site 27) and the unbaked zones (from Site 26) have undergone partial and full remagnetizations. However, because the baked zone granites eventually reach the ChRM of the dyke, we can infer that the original magnetization of the dyke was imprinted on the granitic country rock and the main criteria for a baked contact test is fulfilled (Fig. 6d).

The positive baked contact test from Site 27 strengthens our argument for a northeast shallow primary signal. However, our northeast shallow directions match both the 2.08 Ga and 1.13–1.08 Ga Dharwar Craton magnetizations (e.g., Venkateshwarlu and Chalapathi Rao, 2013; Meert et al., 2021). The trends (NNW-SSE to ENE-WSW) and lithology/texture (diabase/dolerite) of these dykes resemble those of the 2.08 Ga swarm. In contrast, all 1.13–1.08 Ga northeast shallow ChRM directions from the Dharwar Craton are from kimberlite pipes or lamproite dykes and the closest directionally similar dolerite of the same age is the Mahoba dyke of northern India (1.11 Ga; Pradhan et al., 2012; Radhakrishna et al., 2013a). We recognize that detailed statistical treatments and/or geochemical fingerprinting may be necessary to ensure
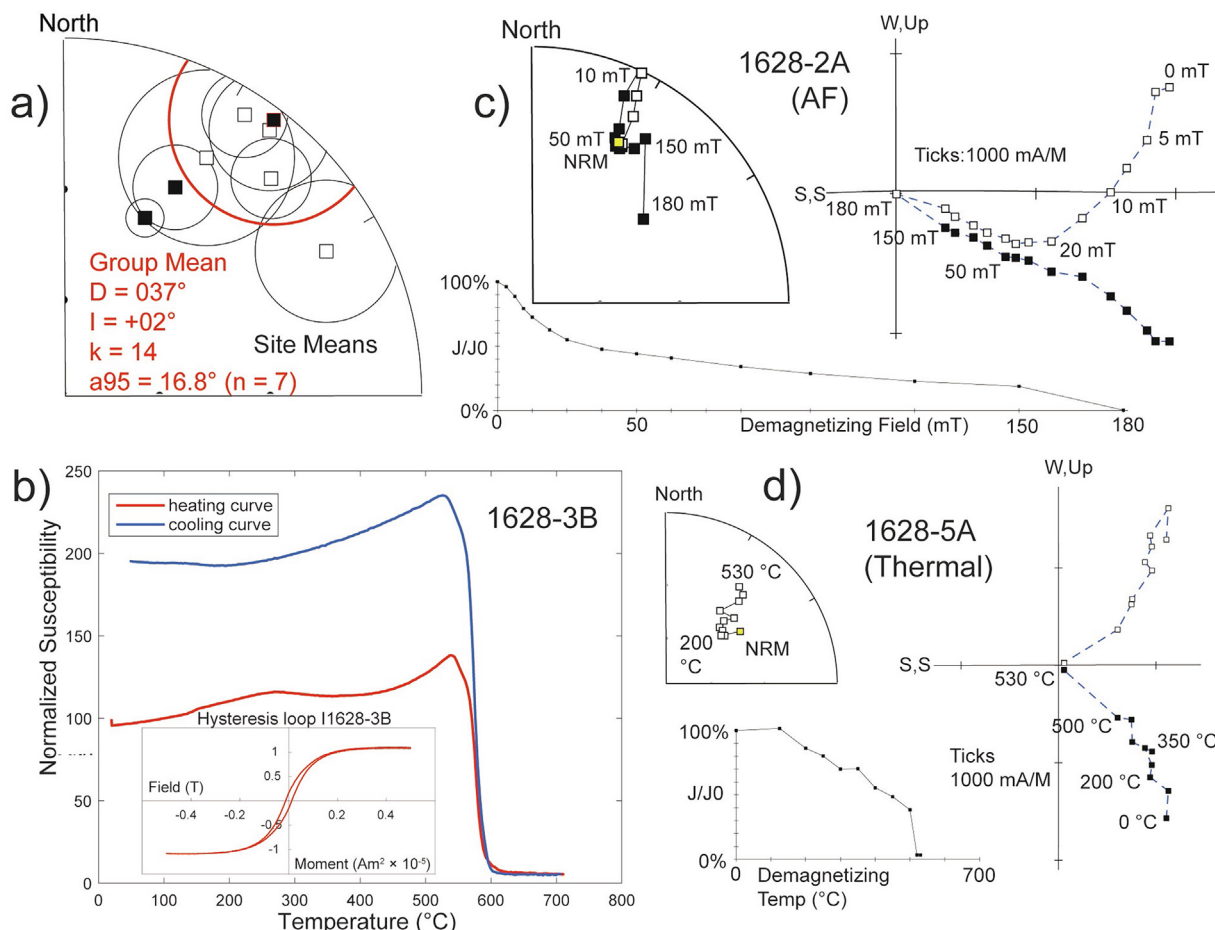
Fig. 5. Demagnetization and rock magnetic results for the northeast shallow group. (a) Individual site means and the northeast shallow group mean. (b) Susceptibility vs temperature curves showing slight alteration on heating and a narrow hysteresis loop for specimen 1628-3B. (c) Two-component AF demagnetization of specimen 1628-2A resolving to the ChRM. (d) Thermal demagnetization of specimen 1628-5A not reaching the ChRM.

the correct swarm assignment. Until then, we consider the common trend and "local" lithology as the best available evidence and tentatively consider the northeast shallow ChRM direction from these dolerite dykes as 2.08 Ga. After inverting all "up" directions ($n = 5$), we calculated a mean VGP for the northeast shallow directional group at 50.4° N, 187.9° E (A95 = 11.8°, $N = 7$), which overlaps within error of the 2.08 Ga Dharwar Craton mean pole at 41° N, 184° E (A95 = 4.6°) from Meert et al. (2021).

3.3. West-northwest shallow directions (1.89–1.86 Ga and 1.79 Ga)

Fourteen dykes (Sites 1, 13–24, 30) with west-northwest shallow up/down directions constitute the majority of sites in our study. Susceptibility vs temperature experiments for these sites indicate the presence of pyrrhotite and/or titanomagnetite along with magnetite as remanence carriers (Fig. 7b, 9c). The wide hysteresis loop for specimen hs1-3c and positive susceptibility beyond 600 °C in Fig. 9c indicates a stronger presence of high coercivity antiferromagnetic minerals (i.e., hematite) than other sites, associated with alteration (perhaps weathering) of the Site 1 dyke.

Sites 15, 19, 22, and 24 exhibited univectorial decay towards west-northwest shallow directions when subjected to thermal and AF demagnetization (Fig. 7c), whereas north shallow down overprints were removed from Sites 13, 14, and 16 and a west-northwest shallow down overprint was removed from Site 21 (Fig. 7d) before reaching the ChRM. We consider the west-

northwest shallow up component isolated at high field/temperature steps (50 mT – 80 mT or 570–600 °C) as the ChRM for the group of sites, yielding a mean direction $D = 282°$, $I = -17°$ (a95 = 6.0°, $k = 53$, $n = 12$) (Fig. 7a). The west-northwest shallow up site mean directions produce a VGP at 9.0° S, 156.7° E, inverted to 9.0° N, 336.7° E (A95 = 5.5°; Fig. 7a, Table 4) that overlaps with VGPs comprising the 1.89–1.86 Ga Dharwar-Bastar mean pole at 34° N 334° E (A95 = 4.5°) from Meert et al. (2021).

Sites 12–18 are in an unnamed drainage channel 4 km south of Devarakonda (Fig. 2b). The large (50-m thick), coarse-grained Site 12 dyke (2.08 Ga) was intruded and baked by ≤ 1 m thick mafic–ultramafic dykes (Sites 13–18), with some intrusions occurring in sub-parallel fashion (trending NE-SW, 050-230°). Ten specimens were drilled from three distinct baked zones of Site 12 as part of three baked contact tests for the intruding Sites 14, 15, and 16, respectively (Fig. 8d). The baked zone specimens from Site 12 showed west-northwest shallow ChRM directions which overlap with ChRM directions of Sites 14, 15, and 16, whereas the unbaked portion of Site 12 yielded a northeast shallow direction (Fig. 8a–c). These directional differences support the preservation of original magnetization for Sites 14, 15, and 16, demonstrating three unambiguous positive baked contact tests for each site and an inverse baked contact test for Site 12 (i.e., that its magnetization is older than that of Sites 14, 15, and 16). The results of the inverse baked contact test support paleomagnetic direction-based age designations for Sites 12 (presumably 2.08 Ga) and Sites 14, 15, and 16 (presumably 1.89–1.86 Ga).
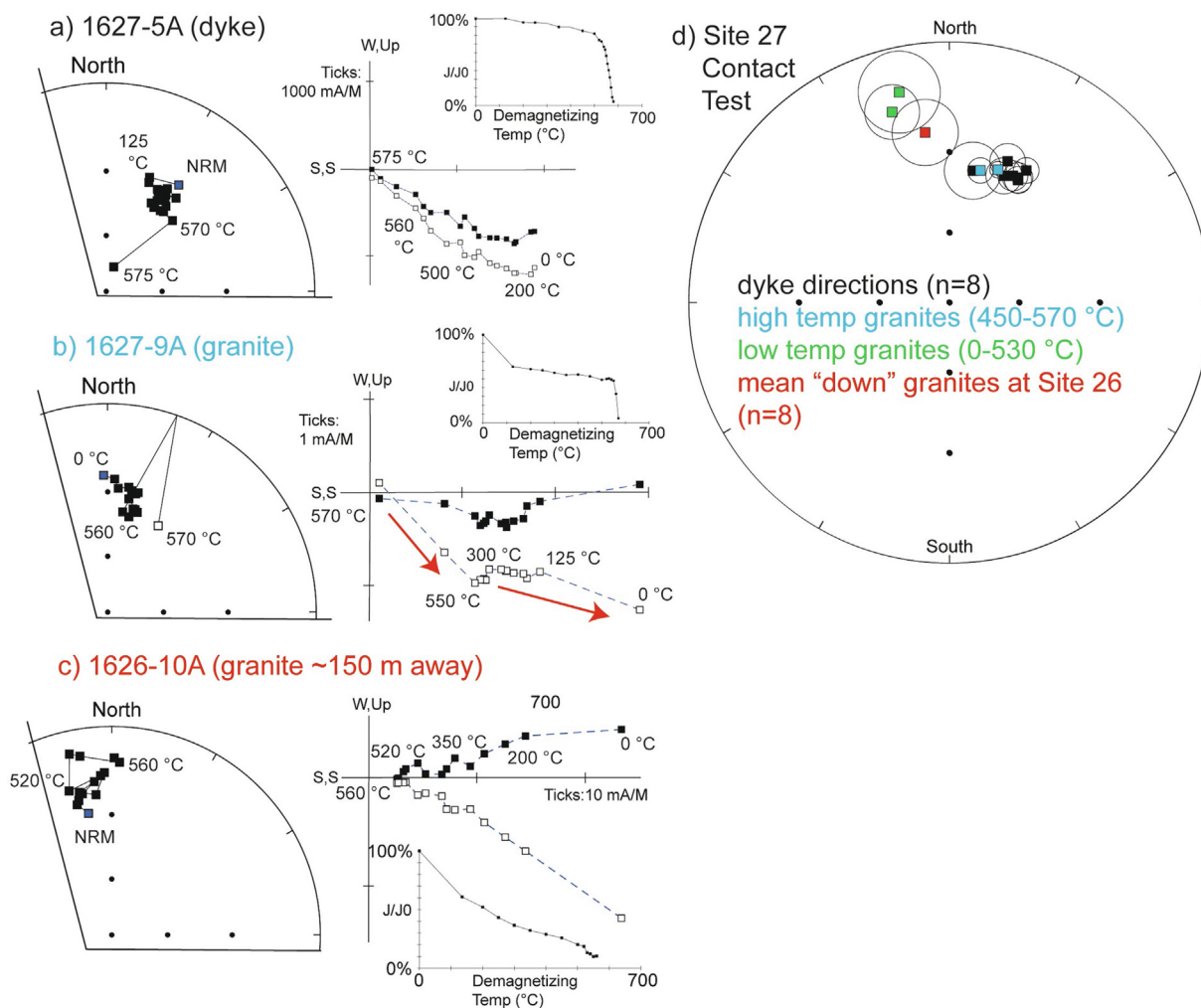
Fig. 6. Baked contact test results for Site 27. Example demagnetizations from the Site 27 dyke (a, black), the Site 27 baked granite (b, blue), and a distant unbaked granite (c, red). In (d) high temperature components of the baked granites match the ChRMs of the Site 27 dykes, while distant unbaked granites and the low temperature components of baked granites (green) exhibit distinct mean directions. (For interpretation of the references to color in this figure legend, the reader is referred to the web version of this article.)

Specimens from Sites 1 and 30 were subject to thermal and AF demagnetization and yielded west-northwest shallow down ChRMs. From Site 30, a low coercivity/temperature north shallow down overprint was removed before isolating the ChRM mean direction $D = 306°$, $I = +15°$ ($a95 = 11.7°$, $k = 16$, $n = 11$; Fig. 9b). Three hand samples (hs1-hs3) from Site 1 showed overlapping demagnetization spectra. Although the directional components of hs3 were distinguishable using both PCA and GCA, hs1 and hs2 directions were only resolvable through GCA (Fig. 9a, b). Specimens from the third (thermal + AF) block yielded a north shallow down low temperature/coercivity component and a northwest moderate down higher temperature/coercivity component at $D = 298°$, $I = +17°$ ($a95 = 5.8°$, $k = 64$, $n = 22$). GCA for all three samples (seven specimens from hs1, six specimens from hs2, eleven specimens from hs3) yielded a mean $D = 284°$, $I = +17°$ (MAD = 17.2°; Fig. 9b), matching the high temperature/coercivity vector isolated in the third block. We chose the PCA-derived high temperature/coercivity component determined from specimens of block 3 as the ChRM for Site 1. The combined means from Sites 1 and 30 yield a mean direction $D = 302°$, $I = +16°$ ($a95 = 16.9°$, $k = 221$) (Fig. 9; Table 5). Given that Site 1 of this study is the 1.79 Ga Pebbair dyke (Söderlund et al., 2019), we report a new 1.79 Ga VGP for these two sites at 33.0° N, 347.5° E.

3.4. Dual polarity moderate-steep directions

Northeast-southwest moderate-steep dual polarity ChRM directions were acquired from six sites (Sites 2, 7, 8, 9, 25, 31; Fig. 10a; Table 6). Susceptibility vs temperature curves indicate magnetite as the primary remanence carrier (Fig. 10b). The sites had consistent within-site thermal demagnetization behavior with ChRMs typically isolated between 450 and 570 °C. Sites 9 and 31 were univectorial with southwest moderate-steep down ChRMs, whereas Sites 2, 7, 8, and 25 exhibited northeast moderate-steep up ChRMs. North shallow down overprints were removed from Sites 2, 7, and 25 by 300–400 °C (Fig. 10a). The north shallow down overprint on these sites resembles the India-wide Ediacaran remagnetization. After inverting Sites 9 and 31, the combined northeast moderate-steep up sites yield a mean ChRM direction $D = 037°$, $I = -59°$ ($a95 = 12.8°$, $k = 28$), which yields a VGP at 23.2° S, 48.3° E ($a95 = 17.8°$, $N = 6$) (Fig. 10; Table 6).

Directional overlap between our northeast-southwest moderate-steep dual polarity sites and several kimberlite pipes without age assignments from the Wajrakarur Kimberlite Field (WKF) and the Narayampet Kimberlite Field (NKF) of the Dharwar Craton by Venkateshwarlu and Chalapathi Rao (2013) suggests that they both belong to the same group (Table 6).
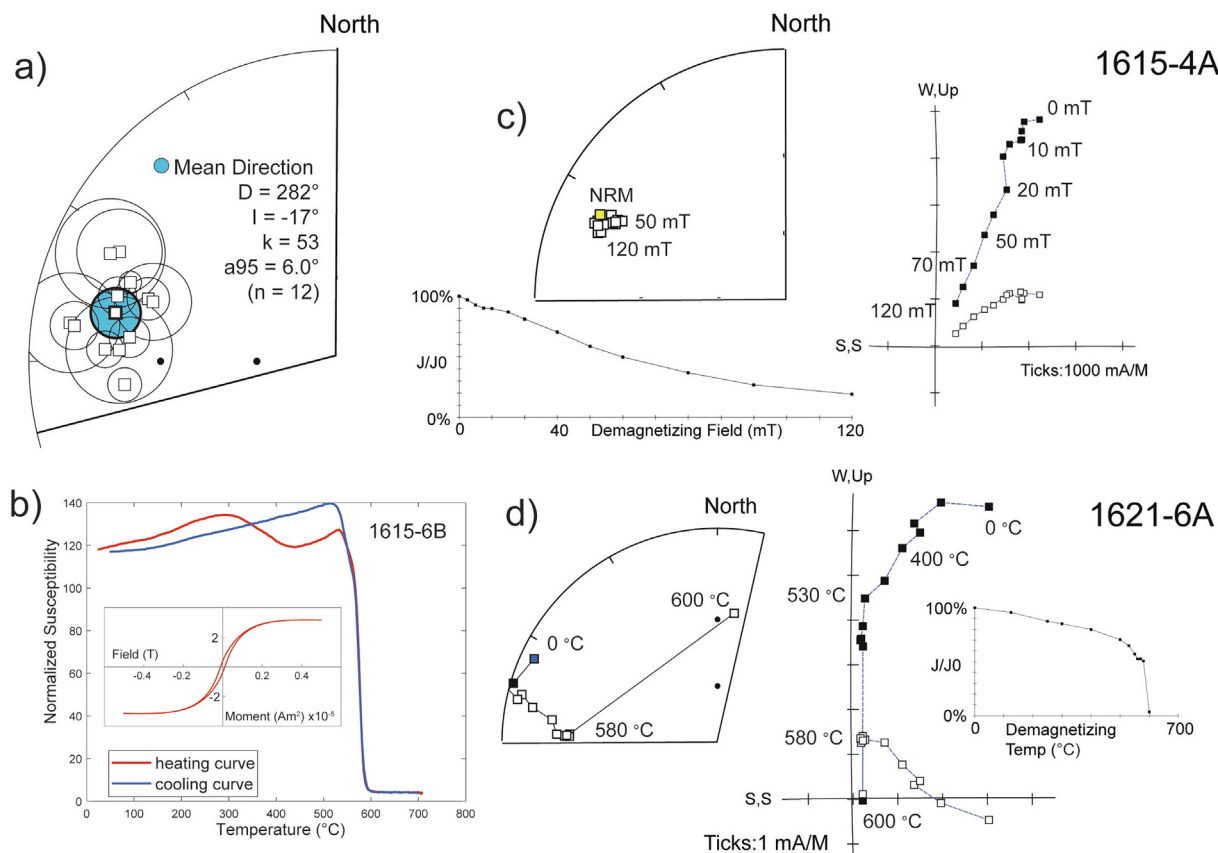
Fig. 7. Demagnetization and rock magnetic results for the west-northwest shallow up group. (a) Individual site means and group mean highlighted in blue. (b) Nearly reversible susceptibility vs temperature curve with alteration on heating and a narrow hysteresis loop for specimen 1615-6B. (c) Univectorial decay in an AF demagnetized specimen 1615-4A. (d) Two-component demagnetization in thermally demagnetized specimen 1621-6A, with a west-northwest shallow down low temperature component. (For interpretation of the references to color in this figure legend, the reader is referred to the web version of this article.)

Poornachandra Rao (2005) identified twenty northeast moderate-steep up directions and one southwest moderate-steep down direction from mafic-ultramafic Dharwar Craton dykes on the edges of the Cuddapah Basin, also matching our data. Although four of these dykes from Poornachandra Rao (2005) are associated with Mesoproterozoic K-Ar and Ar-Ar ages: 1.49 ± 0.04 Ga (J2; K-Ar), 1.37 ± 0.05 Ga (D28; K-Ar), 1.33 ± 0.5 Ga (J15; K-Ar), and 1.21 ± 0.01 Ga (D30; Ar-Ar), analytical details are not provided (Padmakumari and Dayal, 1987; Mallikarjuna et al., 1995). Without $^{40}Ar/^{36}Ar$ ratios to determine the amount of extraneous argon in the dated samples or correlations with other data (e.g., Rb-Sr isotopic data or TiO_2 elemental data), we do not use these dates for comparison with our results (Dalrymple and Lanphere, 1969; Mueller, 1970; Baadsgaard and Mueller, 1973; Kelley, 2002). A combination of directions from the moderate-steep dual polarity sites from this study and the majority of those from Poornachandra Rao (2005) yield a paleomagnetic pole at 20.6° S, 53.1° E, inverted to 20.6° N, 233.1° E (A95 = 9.2°, K = 15, N = 18) (Table 6). The Venkateshwarlu and Chalapathi Rao (2013) sites were excluded from the mean calculation due to low n (n < 4 specimens) and/or high a95 (a95 > 15°) in directional results.

4. U-Pb geochronology results

Table 7 is a summary of notable U-Pb zircon geochronologic results from Site 25 and Site 8 (all results are compiled and tabulated in Supplementary Data S2). Collectively, the U-Pb data from both sites exhibit a wide range of dates, errors, and discordance values, including multiple populations of dates with < 10% discor-

dance. Such issues are common when dating mafic dykes, which are known to incorporate xenocrystic zircon from older cratonic material (country rock or lower crust) and yield discordant dates as a result of open-system behavior (e.g., Black et al., 1991). We follow Schoene et al. (2013) by using the term "ages" when dates can be associated with a geological event (e.g., igneous or metamorphic crystallization). Table 7 also shows that Sites 25 and 8 yield zircons with *meso*-Neoproterozoic U-Pb dates, an interval in which it is often unclear whether $^{238}U/^{206}Pb$ or $^{207}Pb/^{206}Pb$ ratios produce the most accurate and precise crystallization ages for samples globally. Although $^{238}U/^{206}Pb$ system dates typically exhibit lower discordance (percent difference between $^{235}U/^{207}Pb$ and $^{238}U/^{206}Pb$ dates) than $^{207}Pb/^{206}Pb$ system dates (percent difference between $^{207}Pb/^{206}Pb$ and $^{238}U/^{206}Pb$ dates) and are thus preferable for zircons that formed in the younger part of the *meso*-Neoproterozoic, suggestions for a specific "cutoff" boundary vary from ~1.5–0.8 Ga (Russell and Ahrens, 1957; Gehrels, 2000, 2011, 2014; Nemchin and Cawood, 2005; Gehrels et al., 2008; Schoene, 2014; Spencer et al., 2016). The variety of "cutoff" boundaries largely reflects the U contents of the zircons, which result in lower counting errors for higher U grains regardless of their age. Mesoproterozoic and younger geochronological results from Site 25 and Site 8 of this study have lower discordance for $^{238}U/^{206}Pb$ dates than for $^{207}Pb/^{206}Pb$ dates (Table 7). However, within each of our samples, $^{207}Pb/^{206}Pb$ dates are in better agreement with one another than $^{238}U/^{206}Pb$ dates.

Site 25 zircons yielded the following $^{207}Pb/^{206}Pb$ dates from < 10% discordant analyses: (1) an average date of 2.51 ± 0.01 Ga (95% confidence interval) from twenty-two analyses on twenty-
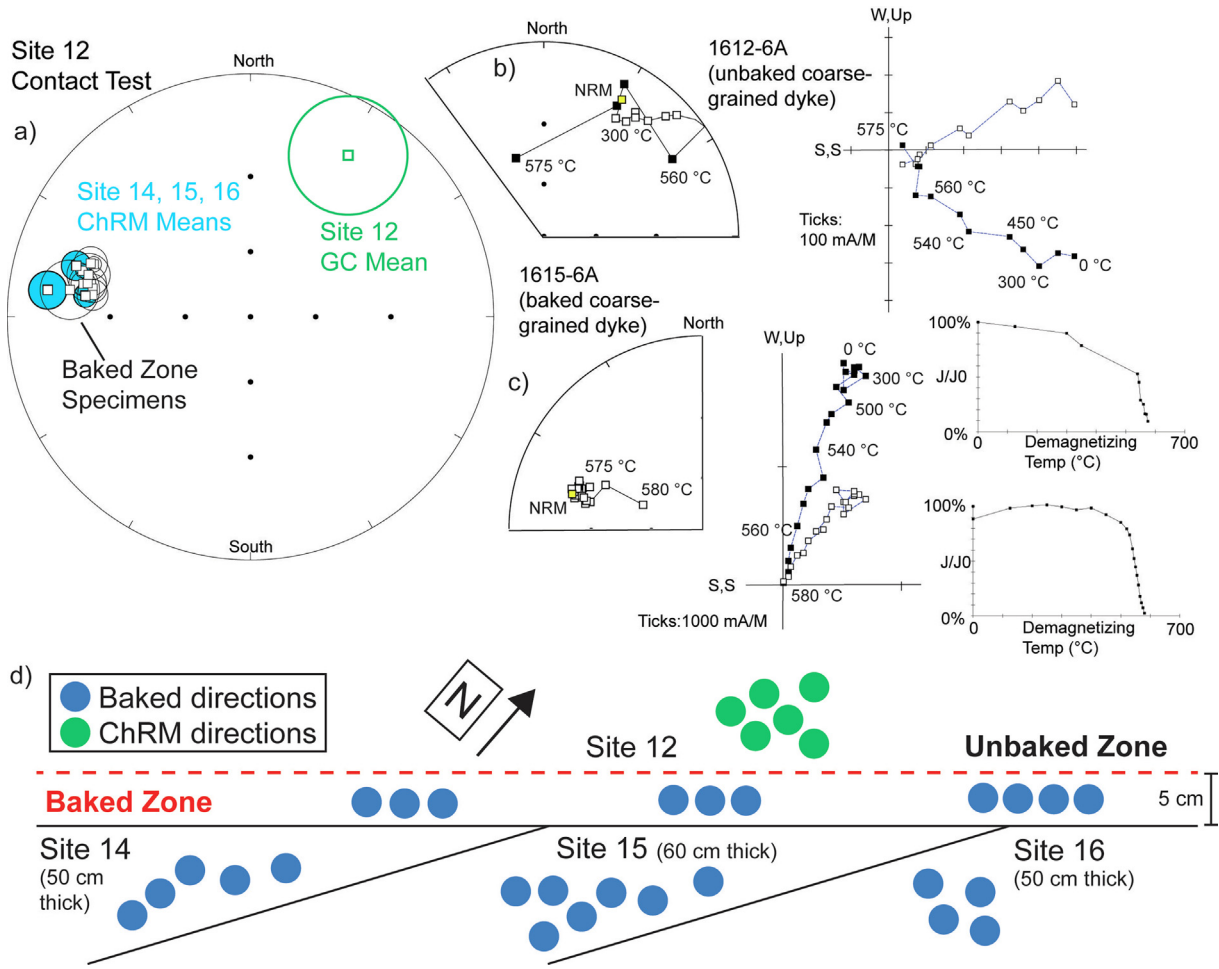
Fig. 8. Baked contact test for Sites 14–16 and inverse baked contact test for Site 12. (a) Stereonet showing Site 14, 15, and 16 ChRM means agreeing with Site 12 baked specimens and distinct from the unbaked Site 12 mean direction. (b–c) Distinct ChRM means determined from the unbaked (b) and baked (c) portions of the coarse-grained dyke. (d) Schematic of dyke relationships in the field (not to scale).
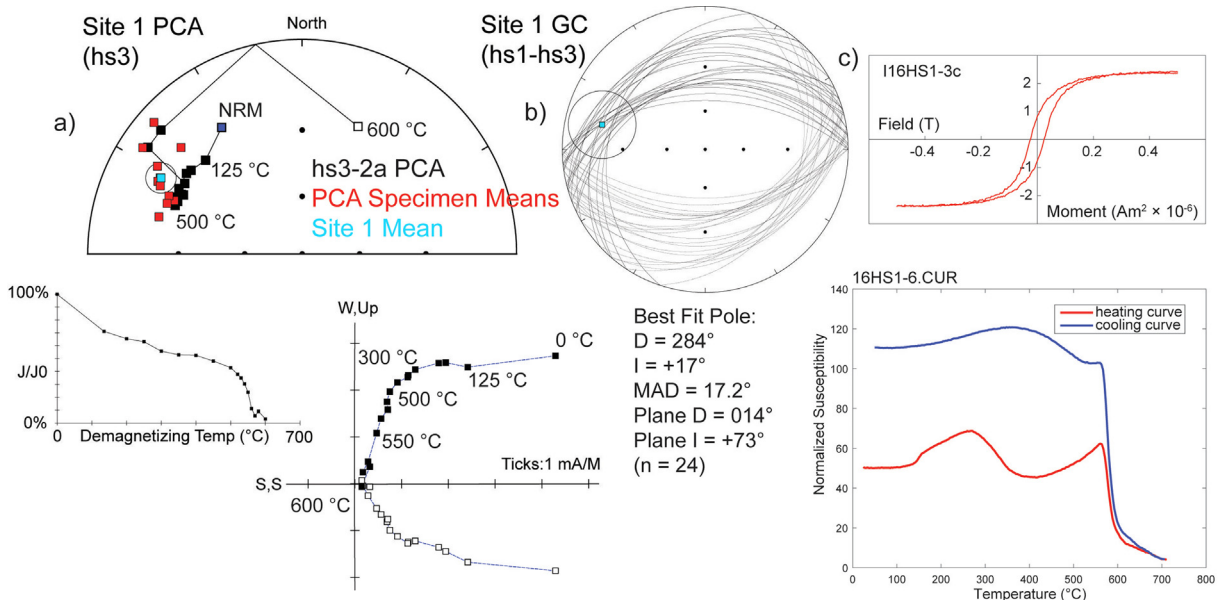
Fig. 9. Demagnetization and rock magnetic results for Site 1 (1.79 Ga). (a) Two component demagnetization of specimen hs3-2a and the west-northwest shallow down PCA-derived site mean. (b) GCA from blocks hs1-hs3 showing a ChRM similar to the PCA-derived site mean. (c) Non-reversible susceptibility vs temperature curves with alteration on heating and a hysteresis loop from specimen hs1-3c.
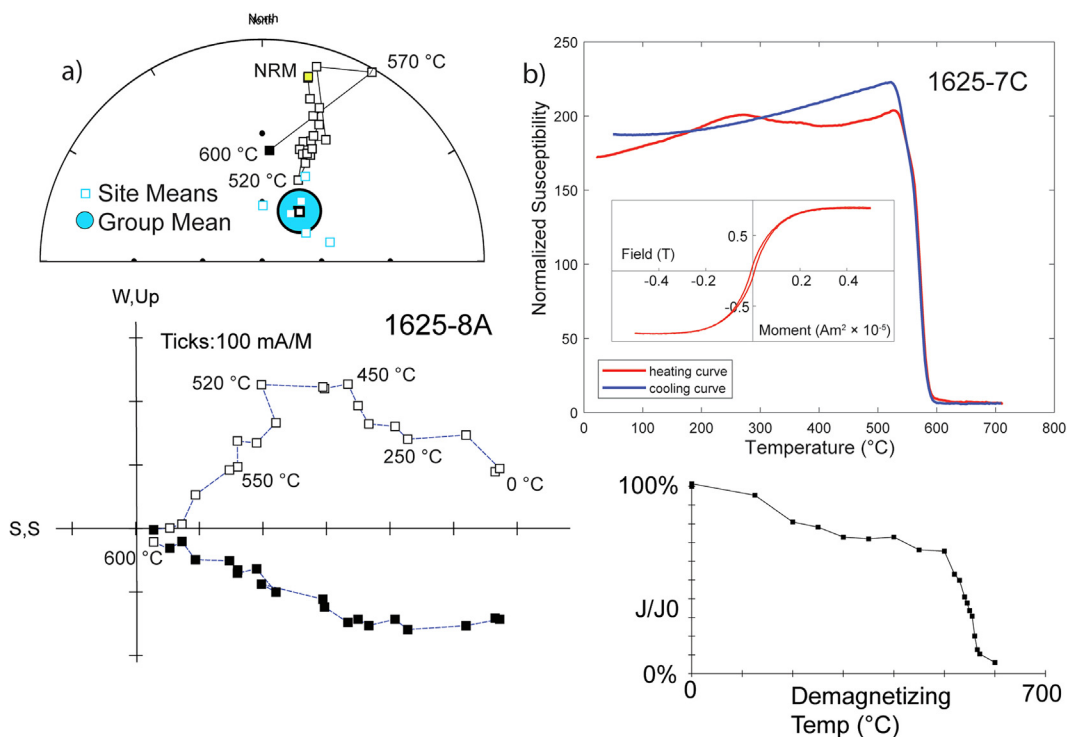
Fig. 10. Demagnetization and rock magnetic results for the northeast-southwest moderate-steep dual polarity group. (a) Specimen 1625-8A showing two-component demagnetization along with other site means and the group mean (after inverting Sites 9 and 31). (b) Reversible susceptibility vs temperature curves with slight alteration on heating and narrow hysteresis for specimen 1625-7C.

Table 2
Steep up directions (2.37 Ga, 2.21 Ga) from dyke sites in this study (abbreviations are as in Table 1).

| Site	Slat (°)	Slong (°)	Trend	N/n	D (°)	I (°)	a95 (°)	k	Plat (°N)	Plong (°E)
5	16.5984	78.0993	10	10	230	−71	4.0	151	35.8	110.4
34	17.5042	78.8689	70	4	83	−73	5.1	–	11.3	47.0

Table 3
Northeast shallow directions (2.08 Ga) from dyke sites in this study (abbreviations are as in Table 1).

Site	Slat (°)	Slong (°)	Trend	N/n	D (°)	I (°)	a95 (°)	k	Plat (°N)	Plong (°E)	A95 (°)
12	16.6539	78.9141	50	5	31	−14	17.2	21	−51.1	24.5	
26	16.6444	78.9012	160	9	33	−4	7.3	50	−52.7	15.7	
27	16.6452	78.9024	60	7	25	33	4.7	167	66.5	162.5	
28	16.6452	78.9024	60	8	28	23	9.4	36	62.3	174.7	
29	16.5473	78.8905	160	3	61	−10	13.2	89	−25.8	3.1	
32	16.6478	78.9036	0	6	38	−4	10.2	44	−48.4	11.6	
33	16.6478	78.9036	spider	5	44	−10	7.5	105	−41.7	11.8	
Mean				7/43	37	2	16.8	14	50.4	187.9	11.8

Table 4
West-northwest shallow up directions (1.89–1.86 Ga) from dyke sites in this study (abbreviations are as in Table 1).

Site	Slat (°)	Slong (°)	Trend	N/n	D (°)	I (°)	a95 (°)	k	Plat (°N)	Plong (°E)	A95 (°)
13	16.6539	78.9141	90	8	288	−24	5.5	103	−13.1	151.3	
14	16.6539	78.9141	90	7	277	−22	5.1	140	−3.3	156.0	
15	16.6539	78.9141	80	15	286	−17	4.5	74	−12.6	155.7	
16	16.6539	78.9141	80	11	278	−9	5.1	82	−6.4	162.5	
17	16.6539	78.9141	80	11	273	−16	4.3	116	−0.5	160.2	
18	16.6539	78.9141	50	8	273	−19	12.9	20	−0.1	158.7	
19	16.6446	78.8712	160	10	264	−20	4.2	133	8.6	160.6	
20	16.6416	78.8767	170	8	296	−13	9.6	34	−22.6	154.2	
21	16.6416	78.8767	115	7	278	−8	10.3	35	−6.6	163.0	
22	16.6416	78.8767	150	6	288	−26	10.1	45	−12.7	150.2	
23	16.6416	78.8767	100	8	295	−12	12.0	22	−21.9	155.1	
24	16.6416	78.8767	150	12	291	−19	2.7	257	−16.9	152.9	
Mean	15	77.5		12/111	282	−17	6.0	53	−9.0	156.7	5.5

Table 5
West-northwest shallow down directions (1.79 Ga) from dyke sites in this study (abbreviations are as in Table 1).

Site	Slat (°)	Slong (°)	Trend	N/n	D (°)	I (°)	a95 (°)	k	Plat (°N)	Plong (°E)	A95 (°)
1	16.2161	77.9960	100	22	298	17	5.8	64	29.3	348.7	
30	16.5473	78.8905	110	11	306	15	11.7	16	36.1	346.2	
Mean				2/33	302	16	16.9	221	33.0	347.5	16.8

Table 6
Northeast-southwest moderate-steep dual polarity directions from dyke sites in this study and previous studies (abbreviations are as in Table 1).

Site	Slat (°)	Slong (°)	Trend	N/n	D (°)	I (°)	a95 (°)	k (K)	Plat (°N)	Plong (°E)	A95 (°)	Refs.
J1	17.4	79.1	15	28	53	−67	10.2	39	−8.3	47.6		1
J2	17.3	79.2	345	30	32	−54	14.4	19	−29.9	49.0		1
K84	16.1	78.1	80	29	20	−66	13.7	26	−23.2	63.8		1
K85	16.1	78.2	0	32	350	−62	11.2	26	−30.0	86.6		1
D11	14.6	77.3	320	31	22	−72	9.7	34	−16.1	65.0		1
D30	14.5	77.8	310	50	51	−64	11.2	22	−14.3	43.8		1
D30A	14.5	77.7	50	37	51	−46	11.4	30	−25.2	28.0		1
DT1	14.9	77.3	55	40	54	−69	12.1	27	−8.2	47.5		1
J15	16.7	79.5	20	36	40	−66	11.1	27	−15.9	53.1		1
D7	14.6	77.4	310	41	339	−77	7.5	70	−8.6	86.1		1
D8	14.7	77.4	70	39	69	−48	6.7	72	−10.4	21.3		1
D62	14.1	77.9	310	41	1	−65	12.9	17	−28.9	77.1		1
2	16.6952	78.0700	0	16	31	−62	3.3	124	−23.7	53.9		2
7	16.8721	78.0228	5	16	33	−54	3.0	148	−29.8	46.9		2
8	16.8143	78.8427	60	17	57	−64	5.9	37	−9.0	42.5		2
9	16.7637	78.9046	130	9	255	55	3.3	251	−2.0	27.0		2
25	16.6451	78.8996	30	15	27	−44	3.6	112	−40.2	46.4		2
31	16.6478	78.9036	170	6	181	62	5.2	164	−30.1	78.2		2
Mean (This Study)				6/79	37	−59	12.8	28	−23.2	48.3	17.8	2
Combined Mean				18/513	36	−63	6.5	29	−20.6	53.1	9.2	2

Notes: Sites 9 and 31 from this study are inverted for the mean calculation. Refs.: 1. Poornachandra Rao (2005), 2. This Study.

Table 7
Selected U-Pb analyses for zircons from Site 25 and Site 8.

	Ratio						Age (Ma)						% Disc.	
Analysis	$^{206}Pb/^{238}U$	1σ	$^{207}Pb/^{235}U*$	$1\sigma*$	$^{207}Pb/^{206}Pb$	1σ	$^{206}Pb/^{238}U$	2σ	$^{207}Pb/^{235}U*$	$2\sigma*$	$^{207}Pb/^{206}Pb$	2σ	7/6	7/5
25-18_R	0.16957	0.00122	1.7406	0.01452	0.07444	0.00031	1010	13	1024	11	1054	17	4.2	1.4
1625s_11	0.15623	0.00177	1.5857	0.01824	0.07361	0.00016	936	20	965	14	1031	9	9.2	3.0
25-23_R	0.08485	0.00082	0.6976	0.00805	0.05962	0.00038	525	10	537	10	590	28	10.9	2.3
25-23_C	0.08141	0.00060	0.6669	0.00711	0.05941	0.00046	505	7	519	9	582	33	13.3	2.7
25-xe^											2514	5		
8-1	0.16219	0.00148	1.6264	0.01668	0.07273	0.00034	969	16	980	13	1006	19	3.7	1.2
8-2	0.23508	0.00217	2.8538	0.02855	0.08805	0.00034	1361	23	1370	15	1383	15	1.6	0.6
8-3	0.15410	0.00144	1.5971	0.01607	0.07517	0.00028	924	16	969	13	1073	15	13.9	4.7
8-4	0.24957	0.00188	3.1450	0.02655	0.09140	0.00035	1436	19	1444	13	1455	14	1.3	0.5
8-5	0.17020	0.00125	1.7306	0.01422	0.07374	0.00027	1013	14	1020	11	1034	15	2.0	0.7

Notes: * indicates that $^{235}U/^{207}Pb$ ratios, ages, and associated 2σ use values of ^{235}U that are calculated from measured ^{238}U. 7/6 = percent discordance for $^{207}Pb/^{206}Pb$ ages, 7/5 = percent discordance for $^{206}Pb/^{238}U$ ages. R = rim, C = core; ^ mean $^{207}Pb/^{206}Pb$ age from Site 25 xenocrysts (*n* = 22 analyses on 21 grains).

one grains, (2) a date of 1.05 ± 0.02 Ga (grain 25–18 rim), and (3) a date of 1.03 ± 0.01 Ga (grain 1625s_11) (Table 7). A core-rim average $^{238}U/^{206}Pb$ date of 0.52 ± 0.01 Ga was calculated for grain 25–23 because the core and rim dates overlap within error (Fig. 11a, b; Table 7). A Wetherill concordia plot of forty-two variably discordant analyses with $^{207}Pb/^{206}Pb$ dates ranging from 2.53 Ga to 2.15 Ga from Site 25 produced upper and lower intercepts at 2.52 ± 0.00 Ga and 0.52 ± 0.01 Ga, respectively, with an MSWD of 4.6 (Fig. 11a; Wetherill, 1956; Silver and Deutsch, 1963) (The upper intercept error of 0.00 Ga is the product of the ISOPLOTR software calculation and was rounded by us to the nearest ten m.y. to match the rest of the contribution – it is unrealistic and the 95% confidence interval should be used instead.). For the ~2.5 Ga modal group from Site 25, BSE and CL images show subhedral-anhedral and subrounded grains with varying degrees of alteration (Fig. 11d–f). < 5% discordant $^{207}Pb/^{206}Pb$ dates were acquired from subhedral, relatively unaltered homogeneous and oscillatory zoned grains (25–29, Fig. 11e) and from highly metam-

ict grains (e.g., 25–12, Fig. 11d; 25–21, Fig. 11f), suggesting closed-system behavior that survived all post-crystallization events for these grains. No concordant dates were acquired from rims of grains with ~2.5 Ga cores. The < 5% discordant 1.05 ± 0.02 Ga date (grain 25–18 rim) is from an overgrowth on a 14% discordant core with a date of 1.35 ± 0.06 Ga (Fig. 11c), suggesting a Mesoproterozoic event affected the country rock.

The Site 25 discordia intercept dates correspond well with the oldest and youngest dates reported for individual zircons, supporting a crystallization age for these grains at 2.52–2.51 Ga and a Pb-loss event at 0.52 Ga that is unrelated to the 1.05–1.03 Ga dates. The Site 25 dyke intrudes ~2.5 Ga granitic country rock (Mukherjee et al., 2018). Thus, the 2.52–2.51 Ga grains likely represent the time of crystallization of the country rock and were xenocrysts in the dyke. A negative correlation between > 2.1 Ga $^{207}Pb/^{206}Pb$ dates and percent discordance also suggests that Pb-loss is the primary reason for discordance (Supplementary Data S2). The existence of 0.52 Ga $^{238}U/^{206}Pb$ dates from grain 25–23

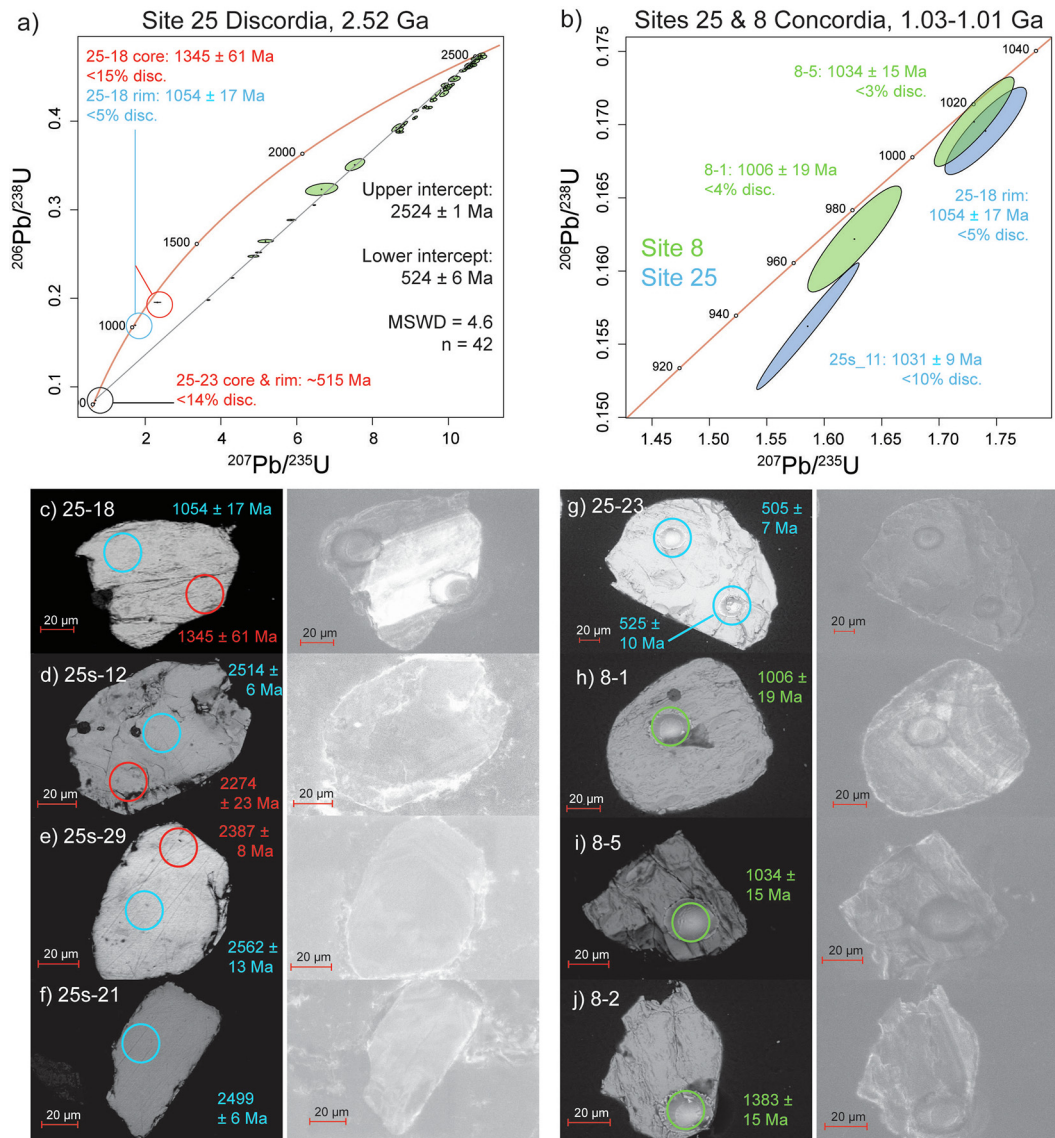**Fig. 11.** U-Pb results from Sites 25 and 8. (a) Discordia for Site 25 with $^{207}Pb/^{206}Pb$ dates for individual analyses. (b) Concordia for Site 25 and Site 8 with $^{207}Pb/^{206}Pb$ dates for individual analyses. (c–j) BSE and CL images of selected grains with $^{207}Pb/^{206}Pb$ ages and spot locations, with blue/green colors indicating a concordant date and red colors indicating a discordant date. In (g) $^{206}Pb/^{238}U$ ages are provided. (For interpretation of the references to color in this figure legend, the reader is referred to the web version of this article.)

suggests that the Pb-loss event was associated with recrystallization or formation of new zircon grains (Fig. 11g). However, Th/U ratios are needed to distinguish between these two possibilities. The 0.52 Ga event associated with Site 25 corresponds to the age of the Kuunga Orogeny, which generated magmatism throughout India during the final assembly of Gondwana (Meert et al., 1995; Meert, 2003; Santosh et al., 2005; Chatterjee et al., 2007; Yin et al., 2010; Grantham et al., 2013; Nanda et al., 2018). As the youngest < 10% discordant analyses that remained unaffected by the Pb-loss event at 0.52 Ga, the 1.05–1.03 Ga analyses ($^{207}Pb/^{206}Pb$) may provide the best constraint for the emplacement age of the Site 25 dyke. Given the lack of absolute age constraints on the "Ediacaran magnetization", it is tempting to suggest that north shallow down magnetic overprints on Site 25 and other sites from this study could be associated with the 0.52 Ga (Lower Cambrian) Pb-loss event. However, Cambrian paleomagnetic directions from India are east and shallow (Davis et al., 2014; Pivarunas et al., 2019). The Site 25 directional overprint therefore suggests either that the "Ediacaran remagnetization" is actually younger than

the Cambrian magnetization (although no extant younger data match this direction), or less likely, that grain 25–23 recrystallized in an environment that did not reset the dyke magnetization.

Site 8 yielded only five zircons, including four < 10% discordant $^{207}Pb/^{206}Pb$ dates at 1.46 ± 0.01 Ga (grain 8–4), 1.38 ± 0.02 Ga (grain 8–2), 1.03 ± 0.02 Ga (grain 8–1), and 1.01 ± 0.02 Ga (grain 8–5) (Fig. 11b, h–j; Table 7). A slightly more discordant (13.9%) analysis yielded a $^{207}Pb/^{206}Pb$ date of 1.07 ± 0.02 Ga. BSE and CL images show oscillatory zoning in grain 8–1 (Fig. 11h), likely indicating igneous crystallization and core-rim overgrowths of indeterminate igneous or metamorphic origins in other grains (Fig. 11i–j). The low number of analyses from Site 8 prohibits the creation of a meaningful discordia and identification of patterns in $^{207}Pb/^{206}Pb$ date vs $^{204}Pb/^{206}Pb$ or $^{207}Pb/^{206}Pb$ date vs percent discordance plots (see Supplementary Data S2). Therefore, we choose the simplest interpretation that the Site 8 dyke was emplaced from 1.03 Ga to 1.01 Ga because it is the youngest and most prevalent age population ($^{207}Pb/^{206}Pb$) from < 10% discordant analyses, and that older grains are xenocrysts. At present, there are no U-Pb zircon/badde-

leyite/perovskite or Pb-Pb baddeleyite ∼1.5–1.3 Ga ages reported for Dharwar Craton mafic dykes. However, 1.44–1.26 Ga Ar-Ar ages exist for lamproite dykes, and this magmatic activity may be related to xenocrysts from Sites 25 and 8 (e.g., Kumar et al., 2021).

Our results for Site 25 and Site 8 exemplify that U-Pb dating of mafic dykes is hindered by the paucity of zircon as an authigenic phase, in addition to xenocryst and discordance problems. Another layer of complication is added for our *meso*-Neoproterozoic zircons because there is no clear choice as to whether $^{238}U/^{206}Pb$ dates or $^{207}Pb/^{206}Pb$ dates are more accurate representations of dyke emplacement ages, especially with a small sample size. Paleomagnetic results support a similar age for the Site 25 and Site 8 dykes that is younger than 2.08 Ga based on a directional overprint on Site 28 (Fig. 5d), although this does little to constrain *meso*-Neoproterozoic crystallization. Considering only < 10% discordant dates, $^{238}U/^{206}Pb$ dates provide a range of 1.01–0.92 Ga (*n* = 5) for Sites 25 and 8 whereas $^{207}Pb/^{206}Pb$ dates provide a more constrained range of 1.05–1.01 Ga (*n* = 4). Because it represents a smaller interval, we assign an age of 1.05–1.01 Ga to the northeast-southwest moderate-steep dual polarity directional group and its accompanying paleomagnetic pole, with acknowledgement that it is a tentative estimate until resolved with more data.

5. Reliability criteria and the Dharwar Craton

Meert et al. (2020) updated the seven quality (Q)-criteria of Van der Voo (1990) for evaluating paleomagnetic datasets and named them reliability (R)-criteria. Based on advancements in analytical technology and thought, and on improvements to the global dataset, the R-criteria are met through more rigorous age requirements and statistical tests than the Q-criteria and provide a clearer outline of best practices for demagnetization techniques. We combine our results from the Dharwar Craton with Proterozoic Indian paleomagnetic poles from previous studies and consider them in the context of the R-criteria (Table 8). The new paleomagnetic poles in Table 8 were calculated using VGP compilations from the main text and in Supplementary Data S3-S9 after applying two filters. The first filter removed VGPs derived from directional results with *n* < 4 specimens and a95 > 15°. The second filter removed anomalous VGPs beyond the Vandamme (1994) cutoff angle. Fig. 12 shows the Proterozoic apparent polar wander paths (APWPs) for Indian cratons color coded by supercontinent association based on the data in Table 8.

Globally, the highest quality poles (*R* = 7) have a presumed rock age that equals the age of magnetization, have averaged paleosecular variation (indicated by sufficient VGP scatter and supported by the presence of reversals), and are tectonically coherent with their host craton (see Meert et al., 2020). In India, the poles that have *R* = 4, 5, or 6 often fall short regarding the first central tenet, which, although expressed through nearly all R-criteria, is most obviously tied to R1 ("radiometric age constrained to within 15 Ma"), R4 ("field tests that constrain magnetization ages"), and R7 ("no resemblance to younger poles by more than a period based on overlapping A95"). However, it is important to note that even if poles have overlapping A95, R7 can be satisfied for the older pole if field tests (R4) constrain magnetization ages (Meert et al., 2020). The spread of radiometric ages in the 2.22–2.21 Ga swarms, the 1.89–1.86 Ga swarms, the 1.13–1.08 Ga kimberlite emplacement, and the 1.05–1.01 Ga swarm of the Dharwar Craton suggest that protracted dyke emplacement over several to perhaps tens of m.y. may be the norm rather than the exception in the Proterozoic Eon. Although this may seem to contradict the rapid emplacement paradigm for LIPs (e.g., Black et al., 2021), dyke emplacement lasted several m.y. after main-phase volcanism in well-

constrained Cenozoic LIP systems such as the Columbia River Basalt Group (cf. Monument dyke swarm to Ice Harbor dyke swarm; Reidel, 2015), and similar systems could have existed in the Proterozoic. Lumping or splitting the Proterozoic Dharwar Craton swarms has important implications for R-scoring, especially when accepting that rock age equals magnetization age (R1, R4, R7).

5.1. The Dharwar Craton and the SIB in the Paleoproterozoic

High quality paleomagnetic poles (with *R*-criteria ≥ 5) are established from the 2.37 Ga, 2.22 Ga, 2.21 Ga, 2.08 Ga, and 1.89–1.86 Ga dyke swarms of the Dharwar Craton (Van der Voo, 1990; Meert et al., 2020, 2021). These poles are derived from large sample sizes with good geochronological control. We add one new VGP to the well-constrained 2.37 Ga Dharwar-Bastar Craton swarm (*R* = 7) and recalculate the mean pole to 11.5° S, 61.0° E (A95 = 4.4°) (Fig. 12; Table 8; Halls et al., 2007; Dash et al., 2013; Pivarunas et al., 2019; Meert et al., 2021). Halls et al. (2007) described the 2.37 Ga swarm as "radiating" and compared its paleomagnetic results with those from the 2.41 Ga Widgiemooltha dykes of the Yilgarn Craton, Australia. Although the 2.37 Ga Dharwar Craton dykes show a variety of trends, the dominant trend is E-W and there is no evidence of a fanning pattern. Based on a more complete paleomagnetic compilation, Belica et al. (2014) argued that age disparities and a 25° latitudinal separation between the Yilgarn Craton and the Dharwar Craton from 2.41 Ga to 2.37 Ga make a linkage unlikely (Evans, 1968; Smirnov et al., 2013). A more recent 2.40 Ga paleomagnetic pole for the Erayinia swarm of the Yilgarn Craton at 22.7° S, 150.5° E (A95 = 11.4°) from Pisarevsky et al. (2015) brings the two cratons to similar latitudes for the time frame, which could substantiate a Yilgarn-SIB connection if the SIB was united (Meert et al., 2021; Pivarunas et al., 2021).

There are no published paleomagnetic results for directly dated dykes of the 2.25 Ga and 2.18 Ga swarms of the Dharwar Craton (French and Heaman, 2010; Nagaraju et al., 2018a; Söderlund et al., 2019). The 2.25 Ga pole from Nagaraju et al. (2018a) was calculated using directional data from dykes adjacent to, and with similar NNW-SSE to NNE-SSW trends as the dated 2.25 Ga dykes. The ∼N—S trend of the 2.25 Ga swarm is identical to the slightly younger 2.22 Ga swarm and VGP overlap is pervasive, producing overlapping A95 confidence intervals for their respective paleomagnetic poles in Fig. 12 (Table 8). The 2.18 Ga pole from Belica et al. (2014) was calculated with directional data from undated dykes. Two such dykes are located near Mahabubnagar, which led Belica et al. (2014) to assign the directions to the 2.18 Ga Mahabubnagar swarm (Pandey et al., 1997). The 2.18 Ga age proposed by Pandey et al. (1997) for these dykes is problematic because it was determined from imprecise whole-rock and mineral Sm-Nd, Rb-Sr, and Pb-Pb isochron ages with errors that overlap with the 2.22 Ga, 2.21 Ga, and 2.08 Ga swarms. French and Heaman (2010) confirmed a 2.18 Ga dyke swarm using U-Pb baddeleyite and zircon analyses, but the closest of these dated dykes is > 200 km to the east of Mahabubnagar near Bandepalem and has no associated paleomagnetic data. Despite these issues, the paleomagnetic directions associated with 2.18 Ga dykes are unique, yielding a paleomagnetic pole at 67.5° N, 84.5° E (A95 = 17.8°, *N* = 4) that is supported by a positive baked contact test (Belica et al., 2014).

Although the NNW-SSE trending 2.22 Ga and WNW-ESE trending 2.21 Ga dyke swarms overlap in age and in site-level VGPs, previous authors have distinguished them through differences in dyke trends and non-overlapping A95 confidence intervals for their mean poles (French and Heaman, 2010; Piispa et al., 2011; Kumar et al., 2012b; Belica et al., 2014; Kumar et al., 2014; Nagaraju et al., 2018a, 2018b; Söderlund et al., 2019; Sarma

Table 8
Selected Proterozoic paleomagnetic poles from India (abbreviations as in Table 1).

Craton	Pole (Ga)	N/n	Slat (°)	Slon (°)	Plat (°)	Plon (°)	A95 (°)	K	Rcalc	Sb (°)	Cut (°)	Rscor	Ref.
Dhar-Bast	2.37	82/663	15.7	77.5	11.5	61.0	4.4	13.6	76.0	22.0	44.6	7	1
Dhar-Bast	2.25	7/53	15.7	77.5	20.2	118.6	12.1	25.9	6.8	14.7	31.5	4	1
Dhar-Bast	2.22	21/218	15.7	77.5	31.5	124.8	7.2	20.4	20.0	17.6	36.7	5	1
Dhar-Bast	2.21	21/216	15.7	77.5	44.0	113.9	9.3	12.6	19.4	22.5	45.5	5	1
Dhar-Bast	2.08	37/416	15.7	77.5	43.1	184.5	4.3	30.7	35.8	14.5	31.1	7	1
Bund	1.98	22/263	25.0	80.0	58.0	309.0	4.8	43.0	21.5	12.1	26.8	6	2
Dhar-Bast	1.89–1.86	72/738	15.7	77.5	19.5	335.7	3.5	23.7	69.0	16.6	34.9	7	1
Dhar-Bast	1.79	2/33	15.7	77.5	33.0	347.5	16.8	–	–	–	–	VGP	1
SIB	1.77	13/183	21.5	86.0	43.3	319.8	10.3	17.3	12.3	18.9	39.0	6	3
SIB	1.79–1.77	11/166	21.5	86.0	38.3	328.3	11.7	16.3	10.4	19.3	39.7	5	1
SIB	1.47	8/60	20.8	82.6	35.7	132.0	15.5	14.0	7.5	16.5	34.7	5	2
SIB	1.15	7/65	20.5	80.3	22.8	28.4	10.8	32.0	6.8	13.2	28.8	5	4
India	1.08	56/500	25.0	79.0	44.4	215.0	3.3	34.0	39.8	14.0	30.2	5	2
India	1.05–1.01	18/513	15.0	77.5	20.6	233.1	9.2	15.1	16.9	20.4	41.7	5	1
India	0.77	28/207	26.0	73.0	68.8	74.0	6.3	19.0	26.6	18.2	37.8	7	2
India	"Ediac."	33/276	15.0	77.5	80.8	280.5	4.2	35.8	32.1	13.3	28.9	3	1

Notes: Rcalc = Length of resultant mean vector (Fisher, 1953), Sb = VGP scatter, Cut = Vandamme (1994) cutoff, Rscor = Reliability Score (Meert et al., 2020). Refs.: 1. This Study; 2. Meert et al., 2021; 3. Pivarunas et al., 2021; 4. De Kock et al., 2015.
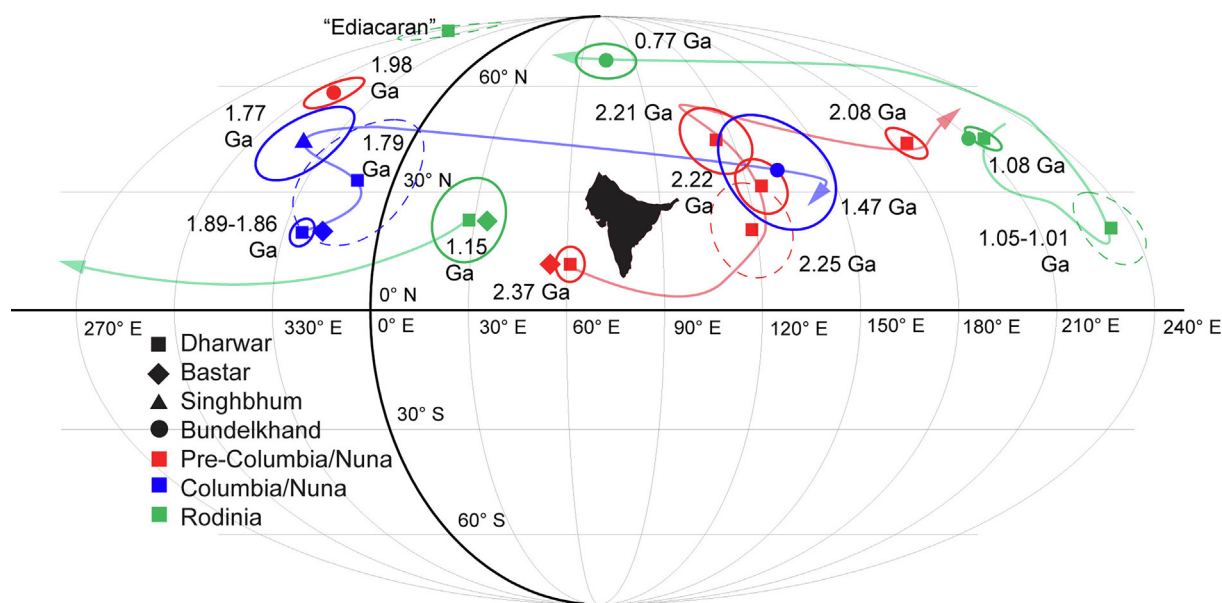

Fig. 12. Newly calculated poles for the Dharwar Craton and India with APWP tracks during supercontinent cycles. Dashed lines indicate poor geochronological control or VGPs.

et al., 2020; Yadav et al., 2020; Meert et al., 2021). However, distinguishing dyke swarms by trend is tenuous and exemplified by slightly overlapping A95 confidence intervals between our filtered 2.22 Ga and 2.21 Ga swarms (Fig. 12; Table 8). The 2.22 Ga and 2.21 Ga poles are controlled by numerous sites collected from the Andhra-Karnataka Long Dyke (AKLD) for the 2.22 Ga swarm and the East-West Long Dyke (EWLD) for the 2.21 Ga swarm. After filtering, these two dykes account for sixteen of twenty-one sites for the 2.22 Ga pole and seven of twenty-one sites for the 2.21 Ga pole (Supplementary Data S5 and S6). The 2.22 Ga swarm has a positive reversals test using the Heslop and Roberts (2018) technique (Nagaraju et al., 2018b; Meert et al., 2021), while the 2.21 Ga swarm lacks a reversal test ("indeterminate" result from Meert et al., 2021). Both swarms lack baked contact tests to constrain ages of magnetization, although Nagaraju et al. (2018b) argued that cross-cutting relations support a magnetization older than 1.89 Ga for the 2.22 Ga directions. The 2.22 Ga and 2.21 Ga mean poles have A95 overlap with the 1.47–1.45 Ga N—S Lakhna dyke swarm pole of the Bastar Craton (Fig. 12; Ratre et al., 2010;

Kumar et al., 2012b; Pisarevsky et al., 2013; Radhakrishna et al., 2013b; Nagaraju et al., 2018b). If the Dharwar and Bastar Cratons were unified at 2.37 Ga (Meert et al., 2021) or 1.88 Ga (e.g., Belica et al., 2014), it poses a problem for the 2.22 Ga and 2.21 Ga swarms regarding resemblance to younger poles (R7 of Meert et al. (2020)). We calculated Bhattacharya coefficients (B (p: q)) and Bayes errors (E^*) for the 2.22 Ga, 2.21 Ga, and 1.47–1.45 Ga poles in Table 8 to quantify their similarities (Heslop and Roberts, 2019). $B(p:q)$ ranges from 0 to 1 with 0 being completely dissimilar and 1 being identical, and (E^*) ranges from 0 to 0.5, with 0 being completely dissimilar and 0.5 being identical. The comparison of 2.22 Ga and 1.47 Ga poles yielded a $B(p:q) = 0.575$ and $E^* = 0.275$, greater than the median value for each parameter, and the probability of a misclassification is 27.5%. Thus, we interpret that the poles are more similar than dissimilar and reduce the 2.22 Ga R rating to $R = 5$. Comparisons between the 2.21 Ga pole and the other two poles yielded smaller $B(p:q) \leq 0.216$ and $E^* \leq 0.101$, suggesting only a 3.2% – 10.1% chance of misclassification. We also evaluated the 2.22 Ga and 2.21 Ga poles according to

the method in Meert and Santosh (2022), who advocated for caution below 20% chance of misclassification. The Bayes error rose slightly to 0.151 (15.1% chance of misclassification) and as a result we keep the 2.21 Ga swarm at $R = 5$.

The 2.08 Ga "radiating" dyke swarm around the Cuddapah Basin is precisely dated with Pb-Pb baddeleyite thermal ionization mass spectrometry (TIMS) ages from eight dykes reported by Kumar et al. (2015) and Söderlund et al. (2019). Meert et al. (2021) calculated a paleomagnetic pole for this swarm (33 sites, 393 samples) at 41° N, 184° E (A95 = 4.6°; $R = 6$). This pole is uniquely located and no coeval swarms from other Indian cratons have been discovered. Our successful baked contact test for the Site 27 dyke indicates the preservation of original magnetization for the northeast shallow directional group. The successful inverse baked contact test for Site 12 further constrains the magnetization age of this group to older than 1.89 Ga. With our new additions, a recalculation for the 2.08 Ga swarm (37 sites, 416 samples) yields a paleomagnetic pole at 43.1° N, 184.5° E (A95 = 4.3°) (Table 8; Piispa et al., 2011; Radhakrishna et al., 2013b; Belica et al., 2014; Kumar et al., 2015). The contact tests promote the R-score for the 2.08 Ga swarm of the Dharwar Craton to $R = 7$.

The 1.89–1.86 Ga swarm(s) of the Dharwar Craton are based on $^{207}Pb/^{206}Pb$ TIMS baddeleyite ages on SE-trending mafic dykes and several mafic sills (French et al., 2008; Belica et al., 2014; Sarma et al., 2020). Belica et al. (2014) also reported a 1.84 Ga U-Pb zircon age from a dyke which they viewed as a minimum age for emplacement. A 1.85 Ga mafic dyke swarm was also reported in the Bastar Craton (French et al., 2008; Shellnutt et al., 2019), but has no associated paleomagnetic data. Parashuramulu et al. (2021) attempted to distinguish 1.89–1.88 Ga and 1.86 Ga dykes of the Dharwar Craton based on differences in polarity. Unfortunately, the only way to ensure that polarity differences between individual dyke sites within a compilation represent distinct periods of dyke emplacement, rather than one longer period which includes multiple magnetic reversals, is to radiometrically date every dyke. Thus, the distinction by Parashuramulu et al. (2021) is arbitrary. Consideration of these data in pole space provides no clear distinction because all VGPs comprising the newly calculated 1.89–1.86 Ga Dharwar-Bastar mean paleomagnetic pole at 19.5° N, 335.7° E (A95 = 3.5°, $N = 72$) lie within the Vandamme (1994) 34.9° VGP cutoff (Table 8). A comprehensive characterization of primary components and overprints from these sites might eventually distinguish these swarms.

Although there is resemblance between the 1.89–1.86 Ga SIB paleomagnetic pole and the 1.79 Ga VGP from dykes of the Dharwar Craton (Fig. 12), positive baked contact tests for the 1.89–1.86 Ga swarm(s) support a primary magnetization. Therefore, the 1.89–1.86 Ga Dharwar-Bastar swarm retains an $R = 7$ (Meert et al., 2020, 2021). Directional data from the 1.89–1.86 Ga Dharwar Craton swarm exhibit a wide swath of site means with ~70° variation in both inclination and declination (after inverting opposite polarity directions and filtering). The swath is large enough to include our west-northwest shallow up and down directional groups. Since the Pebbair dyke is 1.79 Ga, other putative 1.89–1.86 Ga sites may be misclassified, which could explain the wide variation in these data. However, the west-northwest shallow down overprint on a west-northwest shallow up ChRM from Site 21 of this study (Fig. 7d) is consistent with several dykes in the group being > 1.79 Ga. Fig. 12 shows that the 1.79 Ga VGP for the Dharwar Craton slightly overlaps with the 1.77 Ga Singhbhum Craton pole at 43.3° N, 319.8° E (A95 = 10.3°, $N = 13$). The current overlap supports the union of the entire SIB by 1.77 Ga and limited APW for the SIB during the 1.89–1.77 Ga interval. After applying our filter, a 1.79–1.77 Ga SIB pole falls at 38.3° N, 328.3° E (A95 = 11.7°, $N = 11$).

5.2. Mesoproterozoic Indian unity

Mesoproterozoic paleomagnetic poles from the Dharwar Craton are scattered due to limited sampling, inconsistent magnetic directions, and poor geochronologic control (e.g., Anand, 1971; Poornachandra Rao et al., 1984; Miller and Hargraves, 1994). Details of site locations, trends, and demagnetization behavior are also lacking in older studies, resulting in a perplexing array of paleomagnetic directions. However, recent work is filling in gaps in the record. For example, promising 1.44–1.26 Ga Ar-Ar ages exist for lamproite dykes (Kumar et al., 2021), although these dykes lack paleomagnetic data. De Kock et al. (2015) and Wabo et al. (2020, 2022) reported paleomagnetic poles from sedimentary rocks of the Pranhita-Godavari, Chattisgarth, Bhima, and Kaladgi basins (Purana basins) within the SIB. Wabo et al. (2020, 2022) tentatively assigned 1.2–1.1 Ga ages to these poles, although it is unclear whether the stratigraphically correlated sedimentary sequences have Mesoproterozoic or Neoproterozoic depositional ages and magnetization ages. Despite this, Table 8 and Fig. 12 show an example pole at 1.15 Ga. Several high-precision U-Pb Mesoproterozoic ages have been published for Dharwar Craton mafic/ultramafic intrusive units, including the Meda Maarana Halli dyke (of the Harohalli N—S alkaline suite) at 1.19 Ga (Pradhan et al., 2008), the WKF, NKF, and Raichur Kimberlite Field (RKF) at 1.14–1.08 Ga (Chalapathi Rao et al., 2013), and the 1.05–1.01 Ga dyke swarm (this study).

Unfortunately, no paleomagnetic directions were isolated from the dated 1.19 Ga dyke, so Pradhan et al. (2008) combined results from their site I5150 with steep down directions from alkaline dykes studied by Dawson and Hargraves (1994; 2 sites) and Radhakrishna and Mathew (1996; 7 sites) to calculate a 1.19 Ga paleomagnetic pole at 24.9° S, 258° E (A95 = 15°). Despite the large a95 of several site-level VGPs reported by Radhakrishna and Mathew (1996), the Pradhan et al. (2008) grouping produced a uniquely located VGP for the Dharwar Craton. Because the dykes that yielded the paleomagnetic data were not directly dated, Pradhan et al. (2008) urged caution in using these data for paleogeographic reconstructions, although they agree with potentially similar-age poles from De Kock et al. (2015) and Wabo et al. (2020, 2022).

Chalapathi Rao et al. (2013) provided U-Pb ages from perovskite separates from Dharwar Craton kimberlites, including 1.13–1.08 Ga for the WKF (7 pipes), 1.14–1.12 Ga for the NKF (4 pipes), and 1.09 Ga for the RKF (1 pipe). These ages agree with Rb-Sr ages from Kumar et al. (1993, 2001, 2007). Venkateshwarlu and Chalapathi Rao (2013) reported northeast shallow up ChRM directions from four sites from the WKF with a mean $D = 039°, I = -16°$ (a95 = 15.2°, $k = 38$) and a resulting VGP at 44.5° N, 195.4° E. Although none of their paleomagnetic sites were radiometrically dated (M. Venkateshwarlu, National Geophysical Research Institute, written communication, 2020), Venkateshwarlu and Chalapathi Rao (2013) assigned ~1.1 Ga age to the VGP based on the well-constrained 1.13–1.08 Ga ages from Chalapathi Rao et al. (2013). Meert et al. (2021) compiled key poles from the 1.13–1.08 Ga Dharwar kimberlites, the 1.11 Ga Mahoba dyke, the 1.07 Ga Majhgawan Kimberlite, and the ~1.0 Ga Bhander and Rewa sandstones and carbonates of the Bundelkhand Craton to create a 1.08 Ga mean pole for Peninsular India at 44.4° N, 215.0° E (A95 = 3.3°; $R = 5$), which supports a coalescence of Peninsular India by at least ~1.0 Ga (Fig. 12; Table 8; Gregory et al., 2006; Malone et al., 2008; Pradhan et al., 2012; Venkateshwarlu and Chalapathi Rao, 2013; Retallack et al., 2021). The paleomagnetic evidence agrees with the Bhowmik (2019) hypothesis for an ~1.06–0.93 Ga final collision of the NIB and SIB along the CITZ. Bhowmik (2019) argued that the final assembly of the Greater Indian Landmass (GIL) (including NIB and the SIB) occurred

at ~1.0 Ga because of the ubiquity of Grenville-age tectonic events throughout Peninsular India (Roy et al., 2006; Chatterjee, 2018; Chattopadhyay et al., 2020). Such an argument is further supported by multiple Purana Basin closures at ~1.0 Ga (Patranabis-Deb et al., 2007; Malone et al., 2008; Bickford et al., 2011; Mukherjee et al., 2012; Basu and Bickford, 2014, 2015; Patranabis-Deb and Saha, 2020).

The new 1.05–1.01 Ga Dharwar Craton paleomagnetic pole at 20.6° N, 233.1° E (A95 = 9.2°) is distinct from the 1.08 Ga magnetization reported by Meert et al. (2021) in terms of age and pole location (Fig. 12, Table 8). It also suggests that some kimberlites of the WKF and NKF are as young as 1.05–1.01 Ga. The 1.05–1.01 Ga pole satisfies paleosecular variation according to the Deenen et al. (2011, 2014) parameters. Reversal tests were conducted on the dual polarity group, yielding an "indeterminate" result for a common mean using the McFadden and McElhinny (1990) test and weak/ambiguous support for a common mean using the Heslop and Roberts (2018) test that compares populations with different precisions (with Bayes factor = 1.47 and p ($HA|X$) = 0.59). Without applying the directional filter, the Heslop and Roberts (2018) test provides positive support for a common mean for the 1.05–1.01 Ga pole, with Bayes factor = 2.98 and p ($HA|X$) = 0.75 and we accept this result. Lacking relative magnetization age constraints from a baked contact test and absolute age constraints to within ± 15 m.y., the R-score of the 1.05–1.01 Ga pole is 5 (Meert et al., 2020). Because the Meert et al. (2021) pole supports a united India at 1.08 Ga, we present India as a unified block in our Rodinia reconstructions ≤ 1.08 Ga (Fig. 13 and related discussion).

6. India in Columbia

Columbia is Earth's oldest supercontinent whose existence has been invoked through paleomagnetic data, although reports of both a protracted amalgamation and breakup complicate paleogeographic reconstructions (Meert, 2002, 2012; Rogers and Santosh, 2002, 2003, 2004, 2009; Zhao et al., 2002, 2004; Pesonen et al., 2003; Pisarevsky et al., 2003; Hou et al., 2008; Evans and Mitchell, 2011; Evans, 2013; Roberts, 2013; Meert and Santosh, 2017; Elming et al., 2021). No matter the exact age of Columbia's coalescence, it is clear from paleomagnetic results that many continental masses such as Laurentia, Siberia, Baltica, Amazonia, Australia, and the Kalahari Craton formed between ~1.8–1.7 Ga and cannot be considered unified in paleogeographic reconstructions prior to this time (Li, 2000; Evans and Mitchell, 2011; Evans, 2013; Meert and Santosh, 2017; Kirscher et al., 2019). With only two paleomagnetic poles with R ≥ 5 from 1.8 Ga to 1.2 Ga (one from the NIB, the other from the SIB), India's placement in Columbia (and proto-Columbia) reconstructions is speculative.

French et al. (2008) and Shellnutt et al. (2018) outlined the possibility of contiguous LIP(s) at 1.88–1.84 Ga within the Dharwar-Bastar Cratons of India, the Superior Craton of North America, the Kaapvaal Craton (South Africa), and the Yilgarn Craton (Western Australia). While the SIB and the Yilgarn Craton were located at similar latitudes at 1.88 Ga, the rest of the hypothesis lacks support from available paleomagnetic data (Liu et al., 2019; Stark et al., 2019). Zhao et al. (2002, 2003, 2004, 2011) hypothesized a North China-India connection in Columbia based on geochronologic barcoding and contiguity of orogenic belts from ~2.1–1.8 Ga. Whereas 1.77 Ga and ~1.47 Ga poles from the SIB support a SIB-North China connection, there is little evidence for orogenic activity in the CITZ from ~2.1–1.8 Ga (Meert and Santosh, 2017; Bhowmik, 2019; Meert et al., 2021). Pisarevsky et al. (2013, 2014a) placed India adjacent to Baltica from 1.77 Ga to 1.27 Ga based on paleomagnetic results from the Lakhna dykes emplaced from 1.47 Ga to 1.45 Ga
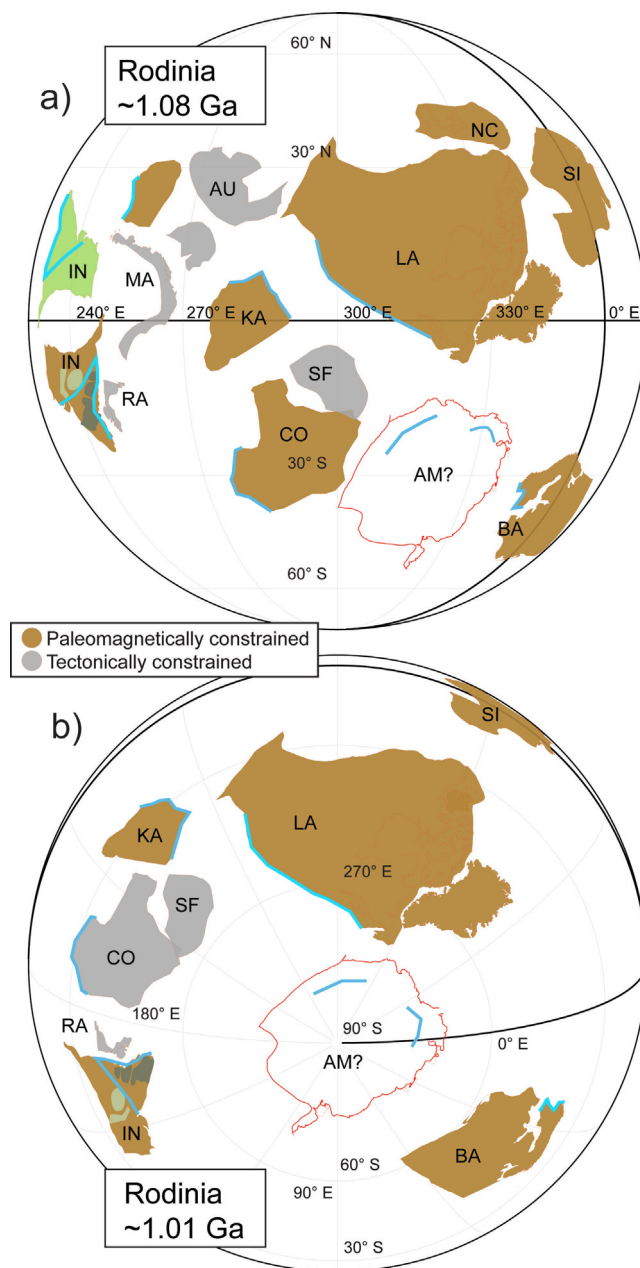

Fig. 13. Rodinia reconstructions at ~1.08 Ga (a) and ~1.01 Ga (b) based on the rotation of paleomagnetic poles in Table 9 to Earth's spin axis using the closest approach method of Meert and Torsvik (2003). For a detailed explanation of Rotation Parameters, see Supplementary Data (S10–S11). AM: Amazonia, AU: Australia, BA: Baltica, CO: Congo, SF: Sao-Francisco, IN: India, KA: Kalahari, LA: Laurentia, MA: Mawson, NC: North China, RA: Rayner, SI: Siberia. Indian Cratons are shaded in light green (NIB) and dark green (SIB). Blue line segments represent orogenic belts for the respective cratons at ~1.1–1.0 Ga (India: Eastern Ghats Mobile Belt; Kalahari Craton: Namaqua-Natal Belt; Baltica: Sveconorwegian orogeny; Australia: Pinjarra orogen; Congo Craton: Lurio, Nampula, and Irumide Belts; Amazon Craton north: Putumayo orogen; Amazon Craton south: Sunsás, Aguapeí and Nova Brasilândia Belts). (a) Rot. Param.: Laurentia: 3.5° N, 268.7° E, 71.2°; Siberia: 54.4° N, 31.3° E, 171.9°; India: 67° N, 207.5° E, 166.2°; inverted India (pole; rotation): −44.4° N, 35° E; 11.7° N, 335° E, 140.7°; Rayner Province: 46° N, 125.5° E, 129.3°; Baltica: 15° N, 290.9° E, −101.3°; Australia (NAC rotated to WAC + SAC): 60.4° N, 75° E, 144.9°; Mawson: 47.8° N, 85.6° E, 158.2°; Kalahari: 5° N, 154.6° E, −156°; Congo: 7.7° N, 331.5° E, −126.7°; Sao Francisco: 4.5° N, 129.5° E, 87.7°; North China: 6.1° N, 45.2° E, 102°; Amazonia: 27.1° N, 113.8° E, 102.2°. (b) Rot. Param.: Laurentia: 0° N, 231.9° E, −122.6°; Baltica: 0° N, 319.8° E, −107.4°; Siberia: 38.7° N, 357.6° E, 140.3°; Congo: 26.1° N, 119.8° E, 136.4°; Kalahari: 46.9° N, 127.8° E, 150.2°; India: 41.3° N, 180.6° E, 98.6°; Amazonia: 39.2° N, 74.8° E, 119.8°; Rayner Province: 18.5° N, 97.8° E, 58.8°. Sao Francisco: 22.8° N, 86.8° E, 130.3°. (For interpretation of the references to color in this figure legend, the reader is referred to the web version of this article.)

(note that there is no evidence India was unified at this time). As in many Columbia reconstructions, Peninsular India is not separated into NIB/SIB in these models and more data are needed to evaluate their accuracy.

7. Rodinia configurations, context and constraints

Rodinia's existence as a supercontinent and its foundational configurations are based largely on global Grenvillian (1.1–1.0 Ga) orogenic correlations between continents (Dalziel, 1991, 1997; Hoffman, 1991, 1999; Moores, 1991; Rogers, 1996; Torsvik et al., 1996; Weil et al., 1998; Condie, 2001; Meert, 2001, 2003; Meert and Powell, 2001; Meert and Torsvik, 2003; Pesonen et al., 2003; Rogers and Santosh, 2003, 2004; Torsvik, 2003; Li et al., 2008, 2013; Bogdanova et al., 2009; Scotese, 2009; Li and Evans, 2011; Evans, 2013, 2021; Zhao et al., 2018a). However, there are many non-unique solutions when aligning any two orogenic belts (Meert, 2014), including the possibility of one or both being created in an Andean-type margin. For example, several formative Rodinia models assumed a connection between India, East Antarctica, and Australia in a long-lived East Gondwana (e.g., Li et al., 1995; Dalziel, 1997; Rogers and Santosh, 2002; Yoshida et al., 2003). Paleomagnetic evidence discredits this hypothesis and even shows that East Antarctica was not fully united until the Ediacaran-Cambrian assembly of greater Gondwana (Powell et al., 1988; Gose et al., 1997; Jones et al., 2003; Meert, 2003, 2014; Meert et al., 2013, 2017). Because Rodinia broke apart between 0.75 Ga and 0.58 Ga, many Rodinia configurations incorporate Neoproterozoic paleomagnetic data, although this does little to constrain Rodinia's arrangement during its formation ~300 m.y. earlier (see refs. above starting with Moores, 1991).

The reliance on Mesoproterozoic-Neoproterozoic paleomagnetic and orogenic correlations from a few key continental blocks (namely Laurentia, Australia, and East Antarctica) produced several "classic" Rodinia configurations (see Li et al., 2008). However, the global Mesoproterozoic paleomagnetic dataset is growing and diversifying, allowing results from previously underrepresented continental blocks to contribute to new hypotheses for Grenvillian orogenic alignments, initial Rodinia arrangements, and periods of true polar wander (Evans, 2003; Zhong et al., 2007; Swanson-Hysell et al., 2019; Evans et al., 2021; Evans et al., 2021; Pesonen et al., 2021). We discuss extant global ~1.1–1.0 Ga data relative to our new India pole at 1.05–1.01 Ga to provide insight into this key interval of Earth's evolution.

7.1. India in Rodinia

Fig. 13 shows possible Rodinia configurations at ~1.08 Ga and ~1.01 Ga. The latitudes of gold-colored continents are paleomagnetically constrained for each time slice, whereas gray-colored continents are constrained through older paleomagnetic and/or geologic (e.g., geochronologic, geochemical, or metamorphic/deformational) affinities presumed to continue through the 1.08–1.01 Ga interval (Table 9). Amazonia lacks a reliable Proterozoic paleomagnetic pole younger than 1.15 Ga, but is often placed adjacent to Laurentia's Grenville margin in Rodinia reconstructions due to geologic affinities which may be non-unique – it is included in Fig. 13 to highlight how its size and presumed central location influences reconstructions (e.g., Loewy et al., 2003; Meert and Torsvik, 2003; Evans, 2013, 2021; Cawood and Pisarevsky, 2017; Slagstad et al., 2017; Ibañez-Mejía, 2020; Martin et al., 2020; D'Agrella-Filho et al., 2021; Nedel et al., 2021; Santo Quadros et al., 2021). The current lack of ~1.1–1.0 Ga paleomagnetic poles from Amazonia, most of Asia, and northern Africa suggest that any

currently published initial Rodinia configuration is subject to improvement. Even Laurentia, which is well constrained for much of the Mesoproterozoic lacks poles in the 1.1–1.0 Ga interval, although it is shown with significant latitudinal movement in Fig. 13 (Swanson-Hysell et al., 2019, Swanson-Hysell, 2021). New Baltica poles shown in Fig. 13 suggest that it was not travelling with Laurentia in its traditional relative orientation at ~1.08 Ga, although the continents occupied similar latitudes by ~1.01 Ga (see fig. 17.3 from Evans et al., 2021; Kulakov et al., 2022). Among the classic Rodinia configurations, the relative orientation of Mawson Craton plus Australia and Laurentia in Fig. 13a most closely resembles an AUSMEX fit (Australia – Mexico; Wingate et al., 2002; Li et al., 2008; Liu et al., 2018).

India is placed on the western periphery of Rodinia in Fig. 13, like the reconstructions of Evans (2021) at 1.05 Ga and Li et al. (2008). However, unlike the Evans (2021) interpretation, Fig. 13b shows India as part of Rodinia at 1.01 Ga. Our newly reported 1.05–1.01 Ga pole shows India at a mid-southerly latitude (~45° S), having moved southward from more equatorial latitudes at 1.08 Ga. This movement is coincident with Laurentia, Siberia, the Kalahari Craton, and the Congo-São Francisco Cratons, supporting hypotheses for Rodinia formation prior to 1.01 Ga (e.g., Swanson-Hysell et al., 2019). It is possible that the formation of Rodinia and one or multiple true polar wander events occurred simultaneously from ~1.08–1.01 Ga (e.g., Evans et al., 2021), but limited data exist for this hypothesis. Assuming a 30–70 m.y. difference between the 1.08 Ga and 1.05–1.01 Ga India poles in Fig. 13 and ~30° of latitudinal difference for India between the two periods, we calculate a minimum velocity range of ~5–11 cm/year for India during this time interval (minimum because longitude is unconstrained).

The CITZ and the Eastern Ghats both have age domains at ~1.0 Ga and are nearly orthogonal, allowing for numerous orientations of India relative to other Grenvillian collisional orogens. The Eastern Ghats are hypothesized to align with the Rayner Province of East Antarctica from 1.05 Ga to 0.95 Ga although the geologic affinities have yet to be supported by paleomagnetic evidence (Fitzsimons, 2000a, 2000b, 2003; Boger, 2011; Harley et al., 2013; Meert et al., 2017). The current extent of the Rayner Province is unknown, and thus it does not significantly influence our paleogeographic reconstructions as an attachment to India in Fig. 13. India has also been proposed as a collisional partner with western Australia during the initial phases of the Pinjarra Orogen ca. 1.08 Ga (e.g., Bruguier et al., 1999; Fitzsimons, 2003; Pisarevsky et al., 2003, 2014b; Boger, 2011). A comparison between both polarity options of the 1.08 Ga all-India pole from Meert et al. (2021) and the 1.07 Ga Bangemall Sills pole of Western Australia from Wingate et al. (2002) in Fig. 13a shows that the Eastern Ghats of India and the Pinjarra orogen of western Australia cannot be aligned, although the CITZ and Pinjarra orogens could be related as distinct segments of a larger suture.

8. Conclusion

The Dharwar Craton of the SIB is intruded by a myriad of Proterozoic mafic dyke swarms that provide geochronologic and paleomagnetic data which together serve as key indicators of its paleogeography. However, these data are not without complication. Our contribution exemplifies that lumping or splitting of different age swarms, resorting to grouping dykes by trend when all other options are exhausted, and applying data filtering techniques all have implications for R-scoring and paleogeography. In the Dharwar Craton alone, there is directional overlap between the 2.37 Ga and 1.05–1.01 Ga swarms, the 2.25 Ga, 2.22 Ga, and 2.21 Ga swarms, the 2.08 Ga and ~1.08 Ga swarms, and the

Table 9
Poles used in Rodinia reconstructions at ~1.08 Ga (Fig. 13a) and ~1.01 Ga (Fig. 13b).

Name	Terrane	Plat (°N)	Plon (°E)	A95 (°)	Age (Ma)	Rscor	Ref.
S—H Bayesian	Laurentia	18.9	181.2	2.6	1080	n/a	Swanson-Hysell et al. (2019)
Haliburton Intrusions	Laurentia	−32.6	141.9	6.3	1015	3 1,110,000	Warnock et al. (2000)
Bamble	Baltica	−6.6	218.4	6.1	1090	3 0,110,010	Kulakov et al. (2022)
Central Telemark	Baltica	−17.4	229.8	6.5	1000	3 0,110,010	Kulakov et al. (2022)
Kartochka	Siberia	19.1	36.3	11.8	1050	5 0,111,101	Gallet et al. (2012); Pisarevsky et al. (2021)
Burovaya Formation	Siberia	−4.5	27.6	–	~1000	3 1,101,000	Pavlov et al. (2019)
All-India	India	44.4	215	3.3	1075	5 0,110,111	Meert et al. (2021)
1.05–1.01 Dharwar	India	20.6	233.1	9.2	1010	5 0,110,111	This Study
Umkondo LIP	Kalahari	−64	222.1	2.6	1110	7 1,111,111	Swanson-Hysell et al. (2015)
Port Edward pluton (inverted)	Kalahari	7.4	147.8	4.2	1010	2 1,010,000	Gose et al. (1997)
Bangemall Sills	W. Australia	33.8	95	8.3	1070	7 1,111,111	Wingate et al. (2002)
Huila-Epembe	Congo	−34.7	256.5	8.7	1110	7 1,111,111	Salminen et al. (2018)
BNFc	North China	−11.2	127.7	8.5	1085	4 0,110,101	Zhao et al. (2020)

1.89–1.86 Ga and 1.79 Ga swarms. Thus, detailed consideration of secondary magnetizations is necessary to defend choices for primary magnetizations and comparison of VGPs is important for removing influential outliers. As datasets grow, statistical tests, rock magnetic data, and geochemical data can play a bigger role in differentiating magnetization events.

Despite these issues, new paleomagnetic poles determined for dykes in this study help refine the role of the Dharwar Craton, the Southern India Block, and Peninsular India in supercontinent reconstructions. The new 1.79 Ga Dharwar Craton VGP overlaps with the 1.77 Ga Singhbhum Craton pole, which sets a minimum time for SIB coalescence. The new 1.05–1.01 Ga pole for the Dharwar Craton contributes to a new reconstruction of Rodinia with India traveling from the equator to higher latitudes with the supercontinent from ~1.08 Ga until at least ~1.01 Ga. Because orogenic alignments are non-unique, our reconstructions in Fig. 13 represent two possible arrangements among many.

CRediT authorship contribution statement

Scott R. Miller: Conceptualization, Data curation, Formal analysis, Investigation, Methodology, Writing – original draft, Writing – review & editing. **Joseph G. Meert:** Conceptualization, Funding acquisition, Investigation, Methodology, Project administration, Supervision, Resources, Software, Writing – review & editing. **Anthony F. Pivarunas:** Conceptualization, Formal analysis, Investigation, Methodology, Software, Writing – review & editing. **Anup K. Sinha:** Investigation, Resources. **Manoj K. Pandit:** Investigation, Resources, Writing – review & editing. **Paul A. Mueller:** Resources, Software, Writing – review & editing. **George D. Kamenov:** Resources, Software, Writing – review & editing.

Declaration of Competing Interest

The authors declare that they have no known competing financial interests or personal relationships that could have appeared to influence the work reported in this paper.

References

Acharyya, S.K., 2003. The nature of Mesoproterozoic Central Indian Tectonic Zone with exhumed and reworked older granulites. Gondwana Res. 6, 197–214.

Anand, S.N., 1971. Geological and geophysical investigations on diamondiferous volcanic pipes from Lattavaram area, Anantapur district, Andhra Pradesh. Geol. Surv. India Miscellaneous Publ. 19, 128–133.

Artemieva, I.M., Mooney, W.D., 2001. Thermal thickness and evolution of Precambrian lithosphere: A global study. J. Geophys. Res.: Solid Earth 106, 16387–16414.

Athavale, R.N., Hansraj, A., Verma, R.K., 1972. Palaeomagnetism and age of Bhander and Rewa sandstones from India. Geophys. J. Int. 28, 499–509.

Baadsgaard, H., Mueller, P.A., 1973. K-Ar and Rb-Sr ages of intrusive Precambrian mafic rocks, southern Beartooth Mountains, Montana and Wyoming. Geol. Soc. America Bull. 84, 3635–3644.

Babu, N.R., Venkateshwarlu, M., Shankar, R., Nagaraju, E., Parashuramulu, V., 2018. New paleomagnetic results on ~ 2367 Ma Dharwar giant dyke swarm, Dharwar craton, southern India: implications for Paleoproterozoic continental reconstruction. J. Earth Syst. Sci. 127, 1–15.

Basu, A., Bickford, M.E., 2014. Contributions of zircon U-Pb geochronology to understanding the volcanic and sedimentary history of some Purāna basins, India. J. Asian Earth Sci. 91, 252–262.

Basu, A., Bickford, M.E., 2015. An alternate perspective on the opening and closing of the intracratonic Purana basins in peninsular India. J. Geol. Soc. India 85, 5–25.

Bazhenov, M.L., Levashova, N.M., Meert, J.G., 2016. How well do Precambrian paleomagnetic data agree with the Phanerozoic apparent polar wander path? A Baltica case study. Precambr. Res. 285, 80–90.

Belica, M.E., Piispa, E.J., Meert, J.G., Pesonen, L.J., Plado, J., Pandit, M.K., Kamenov, G. D., Celestino, M., 2014. Paleoproterozoic mafic dyke swarms from the Dharwar craton; paleomagnetic poles for India from 2.37-1.88 Ga and rethinking the Columbia supercontinent. Precambr. Res. 244, 100–122.

Bhattacharya, A., 2019. Deformation-driven emplacement-differentiation in the Closepet Pluton, Dharwar Craton, South India: an alternative view. Geol. Soc. London Special Publications 489, 261–274.

Bhowmik, S.K., 2019. The current status of orogenesis in the Central Indian Tectonic Zone: a view from its Southern Margin. Geol. J. 54, 2912–2934.

Bhowmik, S.K., Bernhardt, H.J., Dasgupta, S., 2010. Grenvillian age high-pressure upper amphibolite-granulite metamorphism in the Aravalli-Delhi Mobile Belt, Northwestern India: New evidence from monazite chemical age and its implication. Precambr. Res. 178, 168–184.

Bhowmik, S.K., Wilde, S.A., Bhandari, A., Pal, T., Pant, N.C., 2012. Growth of the Greater Indian Landmass and its assembly in Rodinia: Geochronological evidence from Central Indian Tectonic Zone. Gondwana Res. 22, 54–72.

Bhowmik, S.K., Dasgupta, S., Baruah, S., Kalita, D., 2018. Thermal history of a Late Mesoproterozoic paired metamorphic belt (?) during Rodinia assembly: new insight from medium-pressure granulites from the Aravalli-Delhi Mobile Belt, Northwestern India. Geosci. Front. 9, 335–354.

Bickford, M.E., Basu, A., Mukherjee, A., Hietpas, J., Schieber, J., Patranabis-Deb, S., Kumar Ray, R., Guhey, R., Bhattacharya, P., Dhang, P.C., 2011. New U-Pb SHRIMP zircon ages of the Dhamda Tuff in the Mesoproterozoic Chhattisgarh basin, Peninsular India: Stratigraphic implications and significance of a 1-Ga thermal-magmatic event. J. Geol. 119, 535–548.

Bilardello, D., 2019. Civilized magnetist's deadly sins. The IRM Quarterly 28, 1–20.

Black, B.A., Karlstrom, L., Mather, T.A., 2021. The life cycle of large igneous provinces. Nature Rev. Earth & Env. 2, 840–857.

Black, L.P., Kinny, P.D., Sheraton, J.W., 1991. The difficulties of dating mafic dykes: an Antarctic example. Contrib. Mineral. Petrol. 109, 183–194.

Bogdanova, S.V., Pisarevsky, S.A., Li, Z.X., 2009. Assembly and breakup of Rodinia (some results of IGCP Project 440). Strat. and Geol. Corr. 17, 259–274.

Boger, S.D., 2011. Antarctica—before and after Gondwana. Gondwana Res. 19, 335–371.

Bose, S., Dunkley, D.J., Dasgupta, S., Das, K., Arima, M., 2011. India-antarctica-australia-laurentia connection in the Paleoproterozoic-Mesoproterozoic revisited: evidence from new zircon U-Pb and monazite chemical age data from the Eastern Ghats Belt, India. Geol. Soc. America Bull. 123, 2031–2049.

Bruguier, O., Bosch, D., Pidgeon, R.T., Byrne, D.I., Harris, L.B., 1999. U-Pb chronology of the Northampton Complex, Western Australia–evidence for Grenvillian sedimentation, metamorphism and deformation and geodynamic implications. Contrib. Mineral. Petrol. 136, 258–272.

Buchan, K.L., Ernst, R.E., 2021. Plumbing systems of large igneous provinces (LIPs) on Earth and Venus: Investigating the role of giant circumferential and radiating dyke swarms, coronae and novae, and mid-crustal intrusive complexes. Gondwana Res. 100, 25–43.

Cawood, P.A., Pisarevsky, S.A., 2017. Laurentia-baltica-amazonia relations during Rodinia assembly. Precambr. Res. 292, 386–397.

Chadwick, B., Vasudev, V.N., Hegde, G.V., 1997. The Dharwar craton, southern India, and its Late Archean plate tectonic setting: current interpretations and controversies. Proceedings of the Indian Academy of Sciences-Earth and Planetary Sciences 106, 249-258.

Chadwick, B., Vasudev, V.N., Hegde, G.V., 2000. The Dharwar craton, southern India, interpreted as the result of late Archaean oblique convergence. Precambr. Res. 99, 91–111.

Chalapathi Rao, N.V., Wu, F.Y., Mitchell, R.H., Li, Q.L., Lehmann, B., 2013. Mesoproterozoic U-Pb ages, trace element and Sr–Nd isotopic composition of perovskite from kimberlites of the Eastern Dharwar craton, southern India: Distinct mantle sources and a widespread 1.1 Ga tectonomagmatic event. Chem. Geol. 353, 48–64.

Chatterjee, N., 2018. An assembly of the indian shield at c. 1.0 Ga and shearing at 876–764 Ma in Eastern India: insights from contrasting P-T paths, and burial and exhumation rates of metapelitic granulites. Precambr. Res. 317, 117–136.

Chatterjee, N., Mazumdar, A.C., Bhattacharya, A., Saikia, R.R., 2007. Mesoproterozoic granulites of the Shillong-Meghalaya Plateau: evidence of westward continuation of the Prydz Bay Pan-African suture into Northeastern India. Precambrian Res. 152, 1–26.

Chattopadhyay, A., Bhowmik, S.K., Roy, A., 2020. Tectonothermal evolution of the Central Indian tectonic zone and its implications from Proterozoic supercontinental assembly: the current status. Episodes 43, 132–144.

Chaudhuri, A.K., Saha, D., Deb, G.K., Deb, S.P., Mukherjee, M.K., Ghosh, G.I., 2002. The Purana basins of southern cratonic province of India; a case for Mesoproterozoic fossil rifts. Gondwana Res. 5, 23–33.

Chetty, T.R.K., Mohanty, D.P., Yellappa, T., 2012. Mapping of shear zones in the Western Ghats, Southwestern part of Dharwar Craton. J. Geol. Soc. India 79, 151–154.

Condie, K.C., 2001. Continental growth during formation of Rodinia at 1.35-0.9 Ga. Gondwana Res 4, 5–16.

Crawford, A.R., Compston, W., 1973. The age of the Cuddapah and Kurnool systems, southern India. J. Geol. Soc. Australia 19, 453–464.

D'Agrella-Filho, M.S., Antonio, P.Y., Trindade, R.I., Teixeira, W., Bispo-Santos, F., 2021. The Precambrian drift history and paleogeography of Amazonia. In: Pesonen, L.J, Salminen, J., Elming, S.-A., Evans, D., Veikkolainen, T. (Eds.), Ancient Supercontinents and the Paleogeography of Earth. Elsevier, Amsterdam, pp. 207–241.

Dalrymple, G.B., Lanphere, M.A., 1969. Potassium-argon Dating: Principles. Techniques and Applications to Geochronology, Freeman, San Francisco, California, p. 258.

Dalziel, I.W., 1991. Pacific margins of Laurentia and East Antarctica-Australia as a conjugate rift pair: Evidence and implications for an Eocambrian supercontinent. Geology 19, 598–601.

Dalziel, I.W., 1997. OVERVIEW: neoproterozoic-Paleozoic geography and tectonics: Review, hypothesis, environmental speculation. Geol. Soc. America Bull. 109, 16–42.

Dasgupta, S., Sengupta, P., 2003. Indo-Antarctic correlation: a perspective from the Eastern Ghats granulite belt, India. Geol. Soc. Lond. Spec. Publ. 206, 131–143.

Dash, J.K., Pradhan, S.K., Bhutani, R., Balakrishnan, S., Chandrasekaran, G., Basavaiah, N., 2013. Paleomagnetism of ca. 2.3 Ga mafic dyke swarms in the northeastern Southern Granulite Terrain, India: Constraints on the position and extent of Dharwar craton in the Paleoproterozoic. Precambr. Res. 228, 164–176.

Davis, J.K., Meert, J.G., Pandit, M.K., 2014. Paleomagnetic analysis of the Marwar Supergroup, Rajasthan, India and proposed interbasinal correlations. J. Asian Earth Sci. 91, 339–351.

Dawson, E.M., Hargraves, R.B., 1994. Paleomagnetism of Precambrian dike swarms in the Harohalli area, south of Bangalore. India. Precambrian Res. 69, 157–167.

Day, R., Fuller, M., Schmidt, V.A., 1977. Hysteresis properties of titanomagnetites: grain-size and compositional dependence. Phys. Earth Planet. Interiors 13, 260–267.

De Kock, M.O., Beukes, N.J., Mukhopadhyay, J., 2015. Palaeomagnetism of Mesoproterozoic limestone and shale successions of some Purana basins in southern India. Geol. Mag. 152, 728–750.

Deenen, M.H., Langereis, C.G., van Hinsbergen, D.J., Biggin, A.J., 2011. Geomagnetic secular variation and the statistics of palaeomagnetic directions. Geophys. J. International 186, 509-520.

Deenen, M.H., Langereis, C.G., van Hinsbergen, D.J., Biggin, A.J., 2014. Erratum: Geomagnetic secular variation and the statistics of palaeomagnetic directions. Geophys. J. International 197, 643-643.

Demirer, K., 2012. U-Pb baddeleyite ages from mafic dyke swarms in Dharwar craton, India: links to an ancient supercontinent. Ph.D. dissertation, Lund University, p. 25.

Dey, S., Mitra, A., Nandy, J., Mondal, S., Topno, A., Liu, Y., Zong, K., 2019. Chapter 30 - Early crustal evolution as recorded in the Paleoproterozoic of the Singhbhum and Western Dharwar Cratons. In: van Kranendonk, M.J., Kranendonk, M., Bennett, V.C., Elis Hoffmann, J. (Eds.), Earth's Oldest Rocks. Elsevier, pp. 741–792.

Dunlop, D.J., 2002. Theory and application of the Day plot (Mrs/Ms versus Hcr/Hc) 1. Theoretical curves and tests using titanomagnetite data. J. Geophys. Res. Solid Earth 107, EPM-4.

Dunlop, D.J., Özdemir, Ö., 2001. Rock Magnetism: Fundamentals and Frontiers. Cambridge University Press, p. 573.

Dutta, S.K., Vasudevan, K., Chaitra, M.S., Shanker, K., Aggarwal, R.K., 2004. Jurassic frogs and the evolution of amphibian endemism in the Western Ghats. Current Sci. 86, 211–216.

Elming, S.Å., Salminen, J., Pesonen, L.J., 2021. Paleo-Mesoproterozoic Nuna supercycle. In: Pesonen, L.J., Salminen, J., Elming, S.-A., Evans, D., Veikkolainen, T. (Eds.), Ancient Supercontinents and the Paleogeography of Earth. Elsevier, Amsterdam, pp. 499–548.

Eriksson, P.G., Mazumder, R., Catuneanu, O., Bumby, A.J., Ilondo, B.O., 2006. Precambrian continental freeboard and geological evolution: a time perspective. Earth-Sci. Rev. 79, 165–204.

Evans, M.E., 1968. Magnetization of dikes: a study of the paleomagnetism of the Widgiemooltha dike suite, Western Australia. J. Geophys. Res. 73, 3261–3270.

Evans, D.A., 2013. Reconstructing pre-Pangean supercontinents. Geol. Soc. America Bull. 125, 1735–1751.

Evans, D.A., Pesonen, L.J., Eglington, B.M., Elming, S.Å., Gong, Z., Li, Z.X., McCausland, P.J., Meert, J.G., Mertanen, S., Pisarevsky, S.A., Pivarunas, A.F., 2021. An expanding list of reliable paleomagnetic poles for Precambrian tectonic reconstructions. In: Pesonen, L.J, Salminen, J., Elming, S.-A., Evans, D., Veikkolainen, T. (Eds.), Ancient Supercontinents and the Paleogeography of Earth. Elsevier, Amsterdam, pp. 605–639.

Evans, D.A., 2021. Meso-Neoproterozoic Rodinia supercycle. In: Pesonen, L.J., Salminen, J., Elming, S.-A., Evans, D., Veikkolainen, T. (Eds.), Ancient Supercontinents and the Paleogeography of Earth. Elsevier, Amsterdam, pp. 549–576.

Evans, D.A., Mitchell, R.N., 2011. Assembly and breakup of the core of Paleoproterozoic-Mesoproterozoic supercontinent Nuna. Geology 39, 443–446.

Evans, D.A., 2003. True polar wander and supercontinents. Tectonophys. 362, 303-320.

Fisher, R.A., 1953. Dispersion on a sphere. Proceedings of the Royal Society of London. Series A. Math. and Phys. Sci. 217, 295-305.

Fitzsimons, I.C.W., 2000a. A review of tectonic events in the East Antarctic Shield and their implications for Gondwana and earlier supercontinents. J. African Earth Sci. 31, 3–23.

Fitzsimons, I.C.W., 2000b. Grenville-age basement provinces in East Antarctica: evidence for three separate collisional orogens. Geology 28, 879–882.

Fitzsimons, I.C.W., 2003. Proterozoic basement provinces of southern and southwestern Australia, and their correlation with Antarctica. Geol. Soc. Lond. Spec. Publ. 206, 93–130.

French, J.E., Heaman, L.M., 2010. Precise U-Pb dating of Proterozoic mafic dyke swarms fo the Dharwar craton, India: implications for the existence of the Neoproterozoic supercraton Sclavia. Precambr. Res. 183, 416–441.

French, J.E., Heaman, L.M., Chacko, T., Srivastava, R.K., 2008. 1891–1883 Ma Southern Bastar-Cuddapah mafic igneous events, India: A newly recognized large igneous province. Precambr. Res. 160, 308–322.

Friend, C.R.L., Nutman, A.P., 1991. SHRIMP U-Pb geochronology of the Closepet granite and Peninsular gneiss, Karnataka, South India. J. Geol. Soc. India 38, 357–368.

Gallet, Y., Pavlov, V., Halverson, G., Hulot, G., 2012. Toward constraining the long-term reversing behavior of the geodynamo: A new "Maya" superchron ∼1 billion years ago from the magnetostratigraphy of the Kartochka Formation (southwestern Siberia). Earth Planet. Sci. Lett. 339, 117–126.

Gehrels, G.E., 2000. Introduction to detrital zircon studies of Paleozoic and Triassic strata in western Nevada and northern California. Special Paper of the Geol. Soc. America 347, 1–17.

Gehrels, G.E., 2011. Detrital zircon U-Pb geochronology: Current Methods and New Opportunities. In: Busby, C., Azor, A. (Eds.), Tectonics of Sedimentary Basins: Recent Advances. Blackwell Publishing Inc., pp. 45–62.

Gehrels, G.E., 2014. Detrital zircon U-Pb geochronology applied to tectonics. Ann. Rev. Earth Planet. Sci. 42, 127–149.

Gehrels, G.E., Valencia, V.A., Ruiz, J., 2008. Enhanced precision, accuracy, efficiency, and spatial resolution of U-Pb ages by laser ablation–multicollector–inductively coupled plasma–mass spectrometry. Geochem. Geophys. Geosyst. 9, 1–13.

Ghosh, S., D'Souza, J., Goud, B.R., Prabhakar, N., 2022. A review of the Precambrian tectonic evolution of the Aravalli Craton, northwestern India: Structural, metamorphic and geochronological perspectives from the basement complexes and supracrustal sequences. Earth-Sci. Rev. 232, 104098. https://doi.org/10.1016/j.earscirev.2022.104098.

Giri, Y., Radhakrishna, M., Betts, P.G., Biswal, T.K., Armit, R., 2022. Crustal architecture of the Eastern Ghats Mobile Belt: constraints from aeromagnetic, gravity and geological data. Tectonophys 835, 229386. https://doi.org/10.1016/j.tecto.2022.229386.

Gose, W.A., Helper, M.A., Connelly, J.N., Hutson, F.E., Dalziel, I.W., 1997. Paleomagnetic data and U-Pb isotopic age determinations from Coats Land, Antarctica: Implications for late Proterozoic plate reconstructions. J. Geophys. Res.: Solid Earth 102, 7887–7902.

Grantham, G.H., Macey, P.H., Horie, K., Kawakami, T., Ishikawa, M., Satish-Kumar, M., Tsuchiya, N., Graser, P., Azevedo, S., 2013. Comparison of the metamorphic history of the Monapo Complex, northern Mozambique and Balchenfjella and Austhameren areas, Sør Rondane, Antarctica: Implications for the Kuunga Orogeny and the amalgamation of N and S, Gondwana. Precambr. Res. 234, 85–135.

Gregory, L.C., Meert, J.G., Pradhan, V., Pandit, M.K., Tamrat, E., Malone, S.J., 2006. A paleomagnetic and geochronologic study of the Majhgawan kimberlite, India: implications for the age of the Upper Vindhyan Supergroup. Precambr. Res. 149, 65–75.

Grew, E.S., Manton, W.I., 1986. A new correlation of sapphirine granulites in the Indo-Antarctic metamorphic terrain: Late Proterozoic dates from the Eastern Ghats province of India. Precambr. Res. 33, 123–137.

Halls, H.C., 1976. A least-squares method to find a remanence direction from converging remagnetization circles. Geophys. J. Int. 45, 297–304.

Halls, H., 1978. The use of converging remagnetization circles in palaeomagnetism. Phys. Earth Planet. Interiors 16, 1–11.

Halls, H.C., 1982. The importance and potential of mafic dyke swarms in studies of geodynamic processes. Geosci. Canada 9, 145–154.

Halls, H.C., Kumar, A., Srinivasan, R., Hamilton, M.A., 2007. Paleomagnetism and U-Pb geochronology of easterly trending dykes in the Dharwar craton, India: feldspar clouding, radiating dyke swarms and the position of India at 2.37 Ga. Precambr. Res. 155, 47–68.

Harley, S.L., Fitzsimons, I.C., Zhao, Y., 2013. Antarctica and supercontinent evolution: historical perspectives, recent advances and unresolved issues. Geol. Soc. Lond. Spec. Publ. 383, 1–34.

Heslop, D., Roberts, A.P., 2018. Revisiting the paleomagnetic reversal test: a Bayesian hypothesis testing framework for a common mean direction. J. Geophys. Res.: Solid Earth 123, 7225–7236.

Heslop, D., Roberts, A.P., 2019. Quantifying the similarity of paleomagnetic poles. J. Geophys. Res. Solid Earth 124, 12388–12403.

Hoffman, P.F., 1991. Did the breakout of Laurentia turn Gondwanaland inside-out? Science 252, 1409–1412.

Hoffman, P.F., 1999. The break-up of Rodinia, birth of Gondwana, true polar wander and the snowball Earth. J. African Earth Sci. 28, 17–33.

Hou, G., Santosh, M., Qian, X., Lister, G.S., Li, J., 2008. Configuration of the Late Paleoproterozoic supercontinent Columbia: Insights from radiating mafic dyke swarms. Gondwana Res. 14, 395–409.

Huppert, H.E., Sparks, R.S.J., 1985. Cooling and contamination of mafic and ultramafic magmas during ascent through continental crust. Earth Planet. Sci. Lett. 74, 371–386.

Ibañez–Mejía, M., 2020. The Putumayo Orogen of Amazonia: A synthesis. In: Gómez, J., Mateus-Zabala, D. (Eds.), The Geology of Colombia, Volume 1 Proterozoic – Paleozoic. Servicio Geológico Colombiano, pp. 101-131.

Jain, S.C., Nair, K.K.K., Yedekar, D.B., 1995. Geology of the Son-Narmada-Tapti lineament zone in central India. Geol. Surv. India Spec. Publ. 10, 1–154.

Jayananda, M., Martin, H., Peucat, J.J., Mahabaleswar, B., 1995. Late Archaean crust-mantle interactions: geochemistry of LREE-enriched mantle derived magmas. Example of the Closepet batholith, southern India. Contrib. Mineral. Petrol. 119, 314–329.

Jayananda, M., Moyen, J.F., Martin, H., Peucat, J.J., Auvray, B., Mahabaleswar, B., 2000. Late Archaean (2550–2520 Ma) juvenile magmatism in the Eastern Dharwar craton, southern India: constraints from geochronology, Nd–Sr isotopes and whole rock geochemistry. Precambr. Res. 99, 225–254.

Jayananda, M., Tsutsumi, Y., Miyazaki, T., Gireesh, R.V., Kapfo, K.U., Hidaka, H., Kano, T., 2013. Geochronological constraints on Meso-and Neoarchean regional metamorphism and magmatism in the Dharwar craton, southern India. J. Asian Earth Sci. 78, 18–38.

Jayananda, M., Santosh, M., Aadhiseshan, K.R., 2018. Formation of Archean (3600–2500 Ma) continental crust in the Dharwar Craton, southern India. Earth-Sci. Rev. 181, 12–42.

Jones, D.L., Bates, M.P., Li, Z.X., Corner, B., Hodgkinson, G., 2003. Palaeomagnetic results from the ca. 1130 Ma Borgmassivet intrusions in the Ahlmannryggen region of Dronning Maud Land, Antarctica, and tectonic implications. Tectonophys. 375, 247–260.

Kale, V.S., Phansalkar, V.G., 1991. Purana basins of peninsular India: a review. Basin Res. 3, 1–36.

Kelley, S., 2002. K-Ar and Ar-Ar dating. Rev. Mineral. Geochem. 47, 785–818.

Kirscher, U., Liu, Y., Li, Z.X., Mitchell, R.N., Pisarevsky, S.A., Denyszyn, S.W., Nordsvan, A., 2019. Paleomagnetism of the Hart Dolerite (Kimberley, Western Australia)–A two-stage assembly of the supercontinent Nuna? Precambr. Res. 329, 170–181.

Kirschvink, J., 1980. The least-squares line and plane and the analysis of paleomagnetic data. Geophys. J. Int. 62, 699–718.

Klootwijk, C.T., 1973. Palaeomagnetism of upper bhander sandstones from central india and implications for a tentative cambrian gondwanaland reconstruction. Tectonophys 18, 123–145.

Kulakov, E.V., Slagstad, T., Ganerød, M., Torsvik, T.H., 2022. Paleomagnetism and $^{40}Ar/^{39}Ar$ geochronology of meso-neoproterozoic rocks from Southwest Norway. Implications for magnetic remanence ages and the paleogeography of Baltica in a Rodinia supercontinent context. Precambr. Res. 379, 106786. https://doi.org/10.1016/j.precamres.2022.106786.

Kumar, A., Kumari, V.P., Dayal, A.M., Murthy, D.S.N., Gopalan, K., 1993. Rb-Sr ages of Proterozoic kimberlites of India: evidence for contemporaneous emplacement. Precambr. Res. 62, 227–237.

Kumar, A., Gopalan, K., Rao, K.R.P., Nayak, S.S., 2001. Rb-Sr ages of kimberlites and lamproites from Eastern Dharwar craton, South India. J. Geol. Soc. India 58, 135–142.

Kumar, A., Heaman, L.M., Manikyamba, C., 2007. Mesoproterozoic kimberlites in south India: a possible link to~ 1.1 Ga global magmatism. Precambr. Res. 154, 192–204.

Kumar, A., Hamilton, M.A., Halls, H.C., 2012a. A Palaeoproterozoic giant radiating dyke swarm in the Dharwar Craton, southern India. Geochem. Geophys. Geosyst. 13, 1–12.

Kumar, A., Nagaraju, E., Besse, J., Rao, Y.B., 2012b. New age, geochemical and paleomagnetic data on a 2.21 Ga dyke swarm from south India: constraints on Paleoproterozoic reconstruction. Precambr. Res. 220, 123–138.

Kumar, A., Nagaraju, E., Sarma, D.S., Davis, D.W., 2014. Precise Pb baddeleyite geochronology by the thermal extraction-thermal ionization mass spectrometry method. Chem. Geol. 372, 72–79.

Kumar, A., Parashuramulu, V., Nagaraju, E., 2015. A 2082 Ma radiating dyke swarm in the Eastern Dharwar Craton, southern India and its implications to Cuddapah basin formation. Precambr. Res. 266, 490–505.

Kumar, A., Talukdar, D., Rao, N.C., Burgess, R., Lehmann, B., 2021. Mesoproterozoic $^{40}Ar–^{39}Ar$ ages of some lamproites from the Cuddapah Basin and Eastern Dharwar Craton, southern India: implications for diamond provenance of the Banganapalle Conglomerates, age of the Kurnool Group and Columbia tectonics. Geol. Soc. Lond. Spec. Publ. 513, 157–178.

Li, Z.X., 2000. Palaeomagnetic evidence for unification of the North and West Australian cratons by ca. 1.7 Ga: new results from the Kimberley Basin of northwestern Australia. Geophys. J. Int. 142, 173–180.

Li, Z.X., Bobganova, S.V., Collins, A.S., Davidson, A., Waele, B.D., Ernst, R.E., Fitzsimons, I.C.W., Fuck, R.A., Gladkochub, D.P., Jacobs, J., Karlsrom, K.E., Lu, S., Natapov, L.M., Pease, V., Pisarevsky, S.A., Thrane, K., Vernikovsky, V., 2008. Assembly, configuration and break-up history of Rodinia: a synthesis. Precambr. Res. 160, 179–210.

Li, Z.X., Evans, D.A., 2011. Late Neoproterozoic 40 intraplate rotation within Australia allows for a tighter-fitting and longer-lasting Rodinia. Geology 39, 39–42.

Li, Z.X., Zhang, L., Powell, C.M., 1995. South China in Rodinia: part of the missing link between Australia-East Antarctica and Laurentia? Geology 23, 407–410.

Li, Z.X., Evans, D.A., Halverson, G.P., 2013. Neoproterozoic glaciations in a revised global palaeogeography from the breakup of Rodinia to the assembly of Gondwanaland. Sediment. Geol. 294, 219–232.

Li, Z., Zheng, J., Zeng, Q., Liu, Q., Griffin, W.L., 2014. Magnetic mineralogy of pyroxenite xenoliths from Hannuoba basalts, northern North China Craton: implications for magnetism in the continental lower crust. J. Geophys. Res. Solid Earth 119, 806–821.

Liao, A.C.Y., Shellnutt, J.G., Hari, K.R., Denyszyn, S.W., Vishwakarma, N., Verma, C.B., 2019. A petrogenetic relationship between 2.37 Ga boninitic dyke swarms of the Indian Shield: Evidence from the Central Bastar Craton and the NE Dharwar Craton. Gondwana Res. 69, 193–211.

Liu, Y., Li, Z.X., Pisarevsky, S.A., Kirscher, U., Mitchell, R.N., Stark, J.C., Clark, C., Hand, M., 2018. First Precambrian palaeomagnetic data from the Mawson Craton (East Antarctica) and tectonic implications. Sci. Rep. 8, 1–12.

Liu, Y., Li, Z.X., Pisarevsky, S.A., Kirscher, U., Mitchell, R.N., Stark, J.C., 2019. Palaeomagnetism of the 1.89 Ga Boonadgin dykes of the Yilgarn Craton: Possible connection with India. Precambr. Res. 329, 211–223.

Loewy, S.L., Connelly, J.N., Dalziel, I.W., Gower, C.F., 2003. Eastern Laurentia in Rodinia: constraints from whole-rock Pb and U/Pb geochronology. Tectonophys 375, 169–197.

Lowrie, W., 1990. Identification of ferromagnetic minerals in a rock by coercivity and unblocking temperature properties. Geophys. Res. Lett. 17, 159–162.

Magee, C., Ernst, R.E., Muirhead, J., Phillips, T., Jackson, C.A.L., 2019. Magma transport pathways in large igneous provinces: lessons from combining field observations and seismic reflection data. In: Srivastava, R.J., Ernst, R.E., Peng, P. (Eds.), Dyke Swarms of the World: A Modern Perspective. Springer, pp. 45–85.

Mallikarjuna, R.J., Bhattacharji, S., Rao., M.N., Hermes, O.D., 1995. $^{40}Ar–^{39}Ar$ ages and geochemical characteristics of dolerite dykes around the Proterozoic Cuddapah Basin, South India. Geol. Soc. India Memoirs 33, 307-328.

Malone, S.J., Meert, J.G., Banerjee, D.M., Pandit, M.K., Tamrat, E., Kamenov, G.D., Pradhan, V.R., Sohl, L.E., 2008. Paleomagnetism and detrital zircon geochronology of the upper Vindhyan Sequence, Son Valley and Rajasthan, India: A ca. 1000 Ma closure age for the Purana basins? Precambr. Res. 164, 137–159.

Mandal, B., Sen, M.K., Vijaya Rao, V., 2013. New seismic images of the Central Indian Suture Zone and their tectonic implications. Tectonics 32, 908–921.

Martin, E.L., Spencer, C.J., Collins, W.J., Thomas, R.J., Macey, P.H., Roberts, N.M.W., 2020. The core of Rodinia formed by the juxtaposition of opposed retreating and advancing accretionary orogens. Earth-Sci. Rev. 211, 103413. https://doi.org/10.1016/j.earscirev.2020.103413.

Mazumder, R., Bose, P.K., Sarkar, S., 2000. A commentary on the tectono-sedimentary record of the pre-2.0 Ga continental growth of India vis-à-vis a

possible pre-Gondwana Afro-Indian supercontinent. J. Asian Earth Sci. 30, 201–217.

McElhinny, M.W., Cowley, J.A., Edwards, D.J., 1978. Palaeomagnetism of some rocks from Peninsular India and Kashmir. Tectonophys 50, 41–54.

McFadden, P.L., McElhinny, M.W., 1990. Classification of the reversal test in palaeomagnetism. Geophys. J. Int. 103, 725–729.

McKenzie, N.R., Hughes, N.C., Myrow, P.M., Banerjee, D.M., Deb, M., Planavsky, N.J., 2013. New age constraints for the Proterozoic Aravalli-Delhi successions of India and their implications. Precambr. Res. 238, 120–128.

Meert, J.G., 2001. Growing Gondwana and rethinking Rodinia: a paleomagnetic perspective. Gondwana Res. 4, 279–288.

Meert, J.G., 2002. Paleomagnetic evidence for a Paleo-Mesoproterozoic supercontinent Columbia. Gondwana Res. 5, 207–215.

Meert, J.G., 2003. A synopsis of events related to the assembly of eastern Gondwana. Tectonophys. 362, 1–40.

Meert, J.G., 2012. What's in a name? The Columbia (Paleopangaea/Nuna) supercontinent. Gondwana Res. 21, 987–993.

Meert, J.G., 2014. Strange attractors, spiritual interlopers and lonely wanderers: the search for pre-Pangean supercontinents. Geosci. Front. 5, 155–166.

Meert, J.G., Pandit, M.K., 2015. The Archaean and Proterozoic history of Peninsular India: tectonic framework for Precambrian sedimentary basins in India. In: Mazumder, R., Eriksson, P.G. (Eds.), Precambrian Basins of India: Stratigraphic and Tectonic Context. Geol. Soc. London Memoirs 43, 29-54.

Meert, J.G., Pandit, M.K., Pivarunas, A., Katusin, K.D., Sinha, A., 2017. India and Antarctica in the Precambrian: A Brief Analysis. In: Pant, N.C., Dasgupta, S. (Eds.), Crustal Evolution of India and Antarctica: The Supercontinent Connection. Geol. Soc. London Special Publication 457, 339-351.

Meert, J.G., Santosh, M., 2022. The Columbia supercontinent: retrospective, status, and a statistical assessment of paleomagnetic poles used in reconstructions. Gondwana Res. 110, 143–164.

Meert, J.G., Torsvik, T.H., 2003. The making and unmaking of a supercontinent: Rodinia revisited. Tectonophys. 375, 261–288.

Meert, J.G., van der Voo, R., Ayub, S., 1995. Paleomagnetic investigation of the Neoproterozoic Gagwe lavas and Mbozi complex, Tanzania and the assembly of Gondwana. Precambr. Res. 74, 225–244.

Meert, J.G., Pandit, M.K., Pradhan, V.R., Banks, J.C., Sirianni, R., Stroud, M., Newstead, B., Gifford, J., 2010. The precambrian tectonic evolution of India: a 3.0 billion year odyssey. J. Asian Earth Sci. 39, 483–515.

Meert, J.G., Pandit, M.K., Kamenov, G.D., 2013. Further geochronological and paleomagnetic constraints on Malani (and pre-Malani) magmatism in NW India. Tectonophys. 608, 1254–1267.

Meert, J.G., Santosh, M., 2017. The Columbia Supercontinent revisited. Gondwana Res. 50, 67–83.

Meert, J.G., Pivarunas, A.F., Evans, D.A., Pisarevsky, S.A., Pesonen, L.J., Li, Z.X., Elming, S.Å., Miller, S.R., Zhang, S., Salminen, J.M., 2020. The magnificent seven: a proposal for modest revision of the quality index. Tectonophys. 790, 228549. https://doi.org/10.1016/j.tecto.2020.228549.

Meert, J.G., Pivarunas, A.F., Miller, S.R., Pandit, M.K., Sinha, A.K., 2021. The Precambrian drift history and paleogeography of India. In: Pesonen, L.J., Salminen, J., Elming, S.-A., Evans, D., Veikkolainen, T. (Eds.), Ancient Supercontinents and the Paleogeography of Earth. Elsevier, Amsterdam, pp. 305–332.

Meert, J.G., Powell, C.M., 2001. Assembly and break-up of Rodinia: introduction to the special volume. Precambr. Res. 110, 1–8.

Mertanen, S., Halls, H.C., Vuollo, J.I., Pesonen, L.J., Stepanov, V.S., 1999. Paleomagnetism of 2.44 Ga mafic dykes in Russian Karelia, eastern Fennoscandian Shield—implications for continental reconstructions. Precambr. Res. 98, 197–221.

Mezger, K., Cosca, M.A., 1999. The thermal history of the Eastern Ghats Belt (India) as revealed by U-Pb and $^{40}Ar/^{39}Ar$ dating of metamorphic and magmatic minerals: implications for the SWEAT correlation. Precambrian Res. 94, 251–271.

Miller, K.C., Hargraves, R.B., 1994. Paleomagnetism of some Indian kimberlites and lamproites. Precambrian Res. 69, 259–267.

Moores, E.M., 1991. Southwest US-East Antarctic (SWEAT) connection: a hypothesis. Geology 19, 425–428.

Moyen, J.F., Martin, H., Jayananda, M., 2001. Multi-element geochemical modelling of crust–mantle interactions during late-Archaean crustal growth: the Closepet granite (South India). Res. 112, 87–105.

Moyen, J.F., Martin, H., Jayananda, M., Auvray, B., 2003a. Late Archaean granites: a typology based on the Dharwar Craton (India). Precambr. Res. 127, 103–123.

Moyen, J.F., Nédélec, A., Martin, H., Jayananda, M., 2003b. Syntectonic granite emplacement at different structural levels: the Closepet granite, South India. J. Struct. Geol. 25, 611–631.

Mueller, P.A., 1970. TiO$_2$ and K-Ar age: a covariation in the mafic rocks of the Southern Beartooth Mountains of Montana and Wyoming. Earth Planet. Sci. Lett. 9, 427–430.

Mukherjee, A., Bickford, M.E., Hietpas, J., Schieber, J., Basu, A., 2012. Implications of a newly dated ca. 1000-Ma rhyolitic tuff in the Indravati Basin, Bastar Craton, India. J. Geol. 120, 477–485.

Mukherjee, S., Ghosh, G., Das, K., Bose, S., Hayasaka, Y., 2018. Geochronological and geochemical signatures of the granitic rocks emplaced at the north-eastern fringe of the Eastern Dharwar Craton, South India: implications for late Archean crustal growth. Geol. J. 53, 1781–1801.

Nagaraju, E., Parashuramulu, V., Babu, N.R., Narayana, A.C., 2018a. A 2207 Ma radiating mafic dyke swarm from eastern Dharwar craton, Southern India: Drift history through Paleoproterozoic. Precambr. Res. 317, 89–100.

Nagaraju, E., Parashuramulu, V., Kumar, A., Sarma, D.S., 2018b. Paleomagnetism and geochronological studies on a 450 km long 2216 Ma dyke from the Dharwar craton, southern India. Phys. Earth Planet. Interiors 274, 222–231.

Nanda, J., Gupta, S., Hacker, B., 2018. U-Pb zircon and titanite ages from granulites of the Koraput area–evidence for Columbia, Rodinia and Gondwana from the Eastern Ghats Province, India. Precambr. Res. 314, 394–413.

Naqvi, S.M., Rogers, J.J.W., 1983. Precambrian of South India. In: Geol. Soc. India Memoirs, 4. Geological Survey of India, p. 575.

Naqvi, S.M., Rogers, J.J.W., 1987. Precambrian Geology of India. Oxford University Press, Inc., p. 223.

Naqvi, S.M., 2005. Geology and evolution of the Indian plate: From Hadean to Holocene, 4 Ga to 4 Ka. Capital Publishing Company, p. 450.

Nedel, I.M., Fuck, R.A., Ruiz, A.S., Matos-Salinas, G.R., da CD Ferreira, A., 2021. Timing of Proterozoic magmatism in the Sunsas belt, Bolivian Precambrian Shield, SW Amazonian Craton. Geosci. Front. 12, 101247. doi:10.1016/j.gsf.2021.101247.

Nemchin, A.A., Cawood, P.A., 2005. Discordance of the U-Pb system in detrital zircons: implication for provenance studies of sedimentary rocks. Sediment. Geol. 182, 143–162.

Padmakumari, V.M., Dayal, A.M., 1987. Geochronological studies of some mafic dykes around the Cuddapah Basin, South India. In: Radhakrishna, B.P. (Ed.), Purana Basins of Peninsular India. Geol. Soc. India Memoirs 6. Geological Survey of India, pp. 369-374.

Pahari, A., Tang, L., Manikyamba, C., Santosh, M., Subramanyam, K.S.V., Ganguly, S., 2019. Meso-Neoarchean magmatism and episodic crustal growth in the Kudremukh-Agumbe granite-greenstone belt, western Dharwar Craton, India. Precambr. Res. 323, 16–54.

Pandey, B.K., Gupta, J.N., Sarma, K.J., Sastry, C.A., 1997. Sm-Nd, Pb-Pb and Rb-Sr geochronology and petrogenesis of the mafic dyke swarm of Mahbubnagar, South India: implications for Paleoproterozoic crustal evolution of the Eastern Dharwar Craton. Precambr. Res. 84, 181–196.

Pandit, M.K., Pivarunas, A.F., Meert, J.G., 2022. Geochemical and paleomagnetic characteristics of Vestfold Hills mafic dykes in Prydz Bay region: Implications on the Paleoproterozoic connection between East Antarctica and proto-India. Geol. Soc. Lond. Spec. Publ. 518, 149–171.

Parashuramulu, V., Shankar, R., Sarma, D.S., Nagaraju, E., Babu, N.R., 2021. Baddeleyite Pb-Pb geochronology and paleomagnetic poles for ~1.89-1.86 Ga mafic intrusions from the Dharwar craton, India, and their paleogeographic implications. Tectonophys 805, 228789. https://doi.org/10.1016/j.tecto.2021.228789.

Patranabis-Deb, S., Bickford, M.E., Hill, B., Chaudhuri, A.K., Basu, A., 2007. SHRIMP ages of zircon in the uppermost tuff in Chattisgarh basin in central India require~ 500-Ma adjustment in Indian Proterozoic stratigraphy. J. Geol. 115, 407–415.

Patranabis-Deb, S., Saha, S., 2020. Geochronology, paleomagnetic signature and tectonic models of cratonic basins of India in the backdrop of Supercontinent amalgamation and fragmentation. Episodes 43, 145–163.

Pavlov, V.E., Gallet, Y., Petrov, P.Y., 2019. A new Siberian record of the ~ 1.0 Gyr-old Maya superchron. Precambr. Res. 320, 350–370.

Peng, P., Qin, Z., Sun, F., Zhou, X., Guo, J., Zhai, M., Ernst, R.E., 2019. Nature of charnockite and closepet granite in the dharwar craton: implications for the architecture of the archean crust. Precambr. Res. 334, 105478. https://doi.org/10.1016/j.precamres.2019.105478.

Pesonen, L.J., Elming, S.Å., Mertanen, S., Pisarevsky, S., D'Agrella-Filho, M.S., Meert, J. G., Schmidt, P.W., Abrahamsen, N., Bylund, G., 2003. Palaeomagnetic configuration of continents during the Proterozoic. Tectonophys. 375, 289–324.

Pesonen, L.J., Salminen, J., Elming, S.A., Evans, D.A., 2021. In: Veikkolainen, T. (Ed.), Ancient Supercontinents and the Paleogeography of Earth. first ed. Elsevier, Amsterdam, p. 662.

Piispa, E., Smirnov, A.V., Pesonen, L.J., Lingadevaru, M., Murthy, K.A., Devaraju, T.C., 2011. An integrated study of Proterozoic dykes, Dharwar Craton, southern India. In: Srivastava, R.K. (Ed.), Dyke Swarms: Keys for Geodynamic Interpretation. Springer, pp. 33–45.

Pisarevsky, S.A., Gladkochub, D.P., Donskaya, T.V., 2021. Precambrian paleogeography of Siberia. In: Pesonen, L.J., Salminen, J., Elming, S.-A., Evans, D., Veikkolainen, T. (Eds.), Ancient Supercontinents and the Paleogeography of Earth. Elsevier, Amsterdam, pp. 263–275.

Pisarevsky, S.A., Wingate, M.T., Powell, C.M., Johnson, S., Evans, D.A., 2003. Models of Rodinia assembly and fragmentation. Geol. Soc. Lond. Spec. Publ. 206, 35–55.

Pisarevsky, S.A., Biswal, T.K., Wang, X.-C., de Waele, B., Ernst, R., Söderlund, U., Tait, J. A., Ratre, K., Singh, Y.K., Cleve, M., 2013. Paleomagnetic, geochronological and geochemical study of Mesoproterozoic Lakhna dykes in the Bastar craton, India: implications for the Mesoproterozoic supercontinent. Lithos 174, 125–143.

Pisarevsky, S.A., Elming, S.Å., Pesonen, L.J., Li, Z.X., 2014a. Mesoproterozoic paleogeography: Supercontinent and beyond. Precambr. Res. 244, 207–225.

Pisarevsky, S.A., Wingate, M.T., Li, Z.X., Wang, X.C., Tohver, E., Kirkland, C.L., 2014b. Age and paleomagnetism of the 1210 Ma Gnowangerup-Fraser dyke swarm, Western Australia, and implications for late Mesoproterozoic paleogeography. Precambr. Res. 246, 1–15.

Pisarevsky, S.A., De Waele, B., Jones, S., Söderlund, U., Ernst, R.E., 2015. Paleomagnetism and U-Pb age of the 2.4 Ga Erayinia mafic dykes in the south-western Yilgarn, Western Australia: Paleogeographic and geodynamic implications. Precambr. Res. 259, 222–231.

Pivarunas, A.F., Meert, J.G., Pandit, M.K., Sinha, A., 2019. Paleomagnetism and geochronology of mafic dykes from the Southern Granulite Terrane, India: expanding the Dharwar craton southward. Tectonophys. 760, 4–22.

Pivarunas, A.F., Meert, J.G., 2020. Intracratonic stability: a comparison of paleomagnetic data from the north and the south of Dharwar Craton, India. Precambr. Res. 348, 105858.

Pivarunas, A.F., Meert, J.G., Miller, S.R., 2018. Assessing the intersection/remagnetization puzzle with synthetic apparent polar wander paths. Geophys. J. Int. 214, 1164–1172.

Pivarunas, A.F., Meert, J.G., Katusin, K.D., Pandit, M.K., Miller, S.R., Craver, A., Roderus, K.M., Sinha, A., 2021. Paleomagnetic results from the Singhbhum Craton, India: Remagnetization, demagnetization, and complication. Precambr. Res. 359, 106165. https://doi.org/10.1016/j.precamres.2021.106165.

Poornachandra Rao, G.V.S., 2005. Orthogonal dykes around the Cuddapah basin—a paleomagnetic study. J. Indian Geophys. Union 9, 1–11.

Poornachandra Rao, G.S., Murti, C.S., Bhalla, M.S., 1984. Palaeomagnetism of kimberlites around Wajrakarur, Anantapur district, Andhra Pradesh. Geophys. Res. Bull. 22, 105–116.

Powell, C.M., Roots, S.R., Veevers, J.J., 1988. Pre-breakup continental extension in East Gondwanaland and the early opening of the eastern Indian Ocean. Tectonophys 155, 261–283.

Pradhan, V.R., Pandit, M.K., Meert, J.G. 2008, A cautionary note on the age of the paleomagnetic pole obtained from the Harohalli dyke swarms, Dharwar craton, southern India. In: Srivastava, R.K. (Ed.), Indian Dykes. Narosa Publishing House, pp. 339–352.

Pradhan, V.R., Meert, J.G., Pandit, M.K., Kamenov, G., Mondal, M.E.A., 2012. Paleomagnetic and geochronological studies of the mafic dyke swarms of Bundelkhand craton, central India: implications for the tectonic evolution and paleogeographic reconstructions. Precambr. Res. 198, 51–76.

Radhakrishna, B.P., 1987. Purana basins of peninsular India. Geol. Soc. India Memoirs 6. In: Geological Survey of India, p. 518.

Radhakrishna, T., Chandra, R., Srivastava, A.K., Balasubramonian, G., 2013a. Central/Eastern Indian Bundelkhand and Bastar cratons in the Palaeoproterozoic supercontinental reconstructions: A palaeomagnetic perspective. Precambr. Res. 226, 91–104.

Radhakrishna, T., Joseph, M., 1996. Proterozoic palaeomagnetism of the mafic dyke swarms in the high-grade region of southern India. Precambr. Res. 76, 31–46.

Radhakrishna, T., Krishnendu, N.R., Balasubramonian, G., 2013b. Palaeoproterozoic Indian shield in the global continental assembly: evidence from the palaeomagnetism of mafic dyke swarms. Earth-Sci. Rev. 126, 370–389.

Radhakrishna, T., Mathew, J., 1996. Late Precambrian (850–800 Ma) palaeomagnetic pole for the south Indian shield from the Harohalli alkaline dykes: geotectonic implications for Gondwana reconstructions. Precambr. Res. 80, 77–87.

Radhakrishna, B.P., Naqvi, S.M., 1986. Precambrian continental crust of India and its evolution. J. Geol. 94, 145–166.

Ratre, K., De Waele, B., Biswal, T.K., Sinha, S., 2010. SHRIMP geochronology for the 1450 Ma Lakhna dyke swarm: Its implication for the presence of Eoarchaean crust in the Bastar Craton and 1450–517 Ma depositional age for Purana basin (Khariar), Eastern Indian Peninsula. J. Asian Earth Sci. 39, 565–577.

Reidel, S., 2015. Igneous rock associations 15. The Columbia River basalt group: a flood basalt province in the Pacific Northwest, USA. Geosci. Canada 42, 151–168.

Retallack, G.J., Matthews, N.A., Master, S., Khangar, R.G., Khan, M., 2021. Dickinsonia discovered in India and late Ediacaran biogeography. Gondwana Res. 90, 165–170.

Roberts, N.M., 2013. The boring billion? – Lid tectonics, continental growth and environmental change associated with the Columbia supercontinent. Geosci. Front. 4, 681–691.

Rogers, J.J.W., 1986. The Dharwar craton and the assembly of peninsular India. J. Geol. 94, 129–143.

Rogers, J.J.W., 1996. A history of continents in the past three billion years. J. Geol. 104, 91–107.

Rogers, J.J.W., Santosh, M., 2002. Configuration of columbia a mesoproterozoic supercontinent. Gondwana Res. 5, 5–22.

Rogers, J.J.W., Santosh, M., 2003. Supercontinents in Earth history. Gondwana Res. 6, 357–368.

Rogers, J.J.W., Santosh, M., 2004. Continents and Supercontinents. Oxford University Press, p. 289.

Rogers, J.J.W., Santosh, M., 2009. Tectonics and surface effects of the supercontinent Columbia. Gondwana Res. 15, 373–380.

Roy, A., Kagami, H., Yoshida, M., Roy, A., Bandyopadhyay, B.K., Chattopadhyay, A., Khan, A.S., Huin, A.K., Pal, T., 2006. Rb–Sr and Sm–Nd dating of different metamorphic events from the Sausar Mobile Belt, central India: implications for Proterozoic crustal evolution. J. Asian Earth Sci. 26, 61–76.

Russell, R.D., Ahrens, L.H., 1957. Additional regularities among discordant lead-uranium ages. Geochim. Cosmochim. Acta 11, 213–218.

Saha, L., Bhowmik, S.K., Fukuoka, M., Dasgupta, S., 2008. Contrasting episodes of regional granulite-facies metamorphism in enclaves and host gneisses from the Aravalli-Delhi mobile belt, NW India. J. Petrol. 49, 107–128.

Salminen, J., Hanson, R., Evans, D.A., Gong, Z., Larson, T., Walker, O., Gumsley, A., Söderlund, U., Ernst, R., 2018. Direct Mesoproterozoic connection of the Congo and Kalahari cratons in proto-Africa: Strange attractors across supercontinental cycles. Geology 46, 1011–1014.

Samal, A.K., Srivastava, R., 2016. Does geochronology of few dykes of a swarm are representative of all dykes of the same magmatic event? Constraints from the geochemistry and GoogleEarth image, ArcGIS studies of Paleoproterozoic mafic dyke swarms of the Eastern Dharwar craton. Acta Geol. Sin. 90 (S1), 2–3.

Samal, A.K., Srivastava, R.K., Ernst, R.E., Söderlund, U., 2019. Neoarchean-Mesoproterozoic mafic dyke swarms of the Indian Shield mapped using Google Earth™ images and ArcGIS™, and links with large igneous provinces. In: Srivastava, R.K., Ernst, R.E., Peng, P. (Eds.), Dyke Swarms of the World: A Modern Perspective. Springer, pp. 335–390.

Santo Quadros, M.L.D.E., Della Giustina, M.E.S., Rodrigues, J.B., da Silva Souza, V., 2021. Geology and LA-ICP-MS U-Pb geochronology of the Nova Brasilândia belt, SW Amazonian Craton: new ages, re-evaluation of existing geochronological data, and implications for the evolution of the Sunsás orogen. J. South American Earth Sci. 109, 103220. https://doi.org/10.1016/j.jsames.2021.103220.

Santosh, M., Tanaka, K., Yokoyama, K., Collins, A.S., 2005. Late Neoproterozoic-Cambrian felsic magmatism along transcrustal shear zones in southern India: U-Pb electron microprobe ages and implications for the amalgamation of the Gondwana supercontinent. Gondwana Res. 8, 31–42.

Sarkar, S.N., Polkanov, A.A., Gerling, E.K., Chukrov, F.V., 1964. Geochronology of the Precambrians of Peninsular India: a Synopsis. Sci. Cult. 30, 527–537.

Sarma, D.S., Parashuramulu, V., Santosh, M., Nagaraju, E., Babu, N.R., 2020. Pb-Pb baddeleyite ages of mafic dyke swarms from the Dharwar Craton: implications for Paleoproterozoic LIPs and diamond potential of mantle keel. Geosci. Front. 11, 2127–2139.

Schoene, B., 2014. 4.10-U–Th–Pb geochronology. Treat. Geochem. 4, 341–378.

Schoene, B., Condon, D.J., Morgan, L., McLean, N., 2013. Precision and accuracy in geochronology. Elements 9, 19–24.

Scotese, C.R., 2009. Late proterozoic plate tectonics and palaeogeography: a tale of two supercontinents, Rodinia and Pannotia. Geol. Soc. Lond. Spec. Publ. 326, 67–83.

Sengupta, P., Sen, J., Dasgupta, S., Raith, M., Bhui, U.K., Ehl, J., 1999. Ultra-high temperature metamorphism of metapelitic granulites from Kondapalle, Eastern Ghats Belt: implications for the Indo-Antarctic correlation. J. Petrol. 40, 1065–1087.

Shankar, R., Vijayagopal, B., Kumar, A., 2014. Precise Pb–Pb baddeleyite ages of 1765 Ma for a Singhbhum 'newer dolerite' dyke swarm. Current Sci. 106, 1306–1310.

Sharma, R., 2009. Cratons and fold belts of India. In: Reitner, J., Trauth, M.H., Stüwe, K., Yuen, D.A. (Eds.), Lecture Notes in Earth Sciences. Springer, 127, pp. 1–304.

Shellnutt, J.G., Hari, K.R., Liao, A.Y., Denyszyn, S.W., Vishwakarma, N., 2018. A 1.88 Ga giant radiating mafic dyke swarm across southern India and Western Australia. Precambr. Res. 308, 58–74.

Shellnutt, J.G., Hari, K.R., Liao, A.Y., Denyszyn, S.W., Vishwakarma, N., Deshmukh, S. D., 2019. Petrogenesis of the 1.85 Ga sonakhan mafic dyke swarm, bastar craton, India. Lithos 334, 88–101.

Sheth, H.C., Ray, J.S., Ray, R., Vanderkluysen, L., Mahoney, J.J., Kumar, A., Shukla, A.D., Das, P., Adhikari, S., Jana, B., 2009. Geology and geochemistry of Pachmarhi dykes and sills, Satpura Gondwana Basin, central India: problems of dyke-sill-flow correlations in the Deccan Traps. Contrib. Mineral. Petrol. 158, 357–380.

Silver, L.T., Deutsch, S., 1963. Uranium-lead isotopic variations in zircons: a case study. J. Geol. 71, 721–758.

Singh, Y.K., De Waele, B., Karmakar, S., Sarkar, S., Biswal, T.K., 2010. Tectonic setting of the Balaram-Kui-Surpagla-Kengora granulites of the South Delhi Terrane of the Aravalli Mobile Belt, NW India and its implication on correlation with the East African Orogen in the Gondwana assembly. Precambr. Res. 183, 669–688.

Slagstad, T., Roberts, N.M., Kulakov, E., 2017. Linking orogenesis across a supercontinent; the Grenvillian and Sveconorwegian margins on Rodinia. Gondwana Res. 44, 109–115.

Smirnov, A.V., Evans, D.A., Ernst, R.E., Söderlund, U., Li, Z.X., 2013. Trading partners: Tectonic ancestry of southern Africa and western Australia, in Archean supercratons Vaalbara and Zimgarn. Precambr. Res. 224, 11–22.

Söderlund, U., Bleeker, W., Demirer, K., Srivastava, R.K., Hamilton, M., Nilsson, M., Pesonen, L.J., Samal, A.K., Jayananda, M., Ernst, R.E., Srinivas, M., 2019. Emplacement ages of Paleoproterozoic mafic dyke swarms in eastern Dharwar craton, India: implications for paleoreconstructions and support for a∼ 30° change in dyke trends from south to north. Precambr. Res. 329, 26–43.

Spencer, C.J., Kirkland, C.L., Taylor, R.J., 2016. Strategies towards statistically robust interpretations of in situ U-Pb zircon geochronology. Geosci. Front. 7, 581–589.

Srivastava, R.K., Söderlund, U., Ernst, R.E., Mondal, S.K., Samal, A.K., 2019. Precambrian mafic dyke swarms in the Singhbhum craton (eastern India) and their links with dyke swarms of the eastern Dharwar craton (southern India). Precambr. Res. 329, 5–17.

Srivastava, R.K., Söderlund, U., Ernst, R.E., Gautam, G.C., 2021. A ca. 2.25 Ga mafic dyke swarm discovered in the Bastar craton, Central India: Implications for a widespread plume-generated large Igneous Province (LIP) in the Indian shield. Precambr. Res. 360, 106232. https://doi.org/10.1016/j.precamres.2021.106232.

Stark, J.C., Wang, X.C., Denyszyn, S.W., Li, Z.X., Rasmussen, B., Zi, J.W., Sheppard, S., Liu, Y., 2019. Newly identified 1.89 Ga mafic dyke swarm in the Archean Yilgarn Craton, Western Australia suggests a connection with India. Precambr. Res. 329, 156–169.

Steiger, R.H., Jäger, E., 1977. Subcommission on geochronology: convention on the use of decay constants in geo- and cosmochronology. Earth Planet. Sci. Lett. 36, 359–362.

Storey, B.C., 1995. The role of mantle plumes in continental breakup: case histories from Gondwanaland. Nature 377, 301–308.

Swanson-Hysell, N.L., 2021. The Precambrian paleogeography of Laurentia. In: Pesonen, L.J., Salminen, J., Elming, S.-Å., Evans, D., Veikkolainen, T. (Eds.), Ancient Supercontinents and the Paleogeography of Earth. Elsevier, Amsterdam, pp. 109–153.

Swanson-Hysell, N.L., Kilian, T.M., Hanson, R.E., 2015. A new grand mean palaeomagnetic pole for the 1.11 Ga Umkondo large igneous province with implications for palaeogeography and the geomagnetic field. Geophys. Suppl. Monthly Notices R. Astronom. Soc. 203, 2237–2247.

Swanson-Hysell, N.L., Ramezani, J., Fairchild, L.M., Rose, I.R., 2019. Failed rifting and fast drifting: Midcontinent rift development, Laurentia's rapid motion and the driver of Grenvillian orogenesis. Geol. Soc. America Bull. 131, 913–940.

Tauxe, L., 2010. Essentials of Paleomagnetism, third. University of California Press, Berkeley, p. 512.

Torsvik, T.H., 2003. The Rodinia jigsaw puzzle. Science 300, 1379–1381.

Torsvik, T.H., Smethurst, M.A., Meert, J.G., Van der Voo, R., McKerrow, W.S., Brasier, M.D., Sturt, B.A., Walderhaug, H.J., 1996. Continental break-up and collision in the Neoproterozoic and Palaeozoic—a tale of Baltica and Laurentia. Earth-Sci. Rev. 40, 229–258.

Torsvik, T.H., Doubrovine, P., Domeier, M., 2016. Interactive analysis of paleomagnetic data software. Ivar Giaver Geomagnetic Laboratory.

Turcotte, D.L., Schubert, G., 2002. Geodynamics. Cambridge University Press, New York, p. 472.

Van der Voo, R., 1990. The reliability of paleomagnetic data. Tectonophys. 184, 1-9.

Vandamme, D., 1994. A new method to determine paleosecular variation. Phys. Earth Planet. Interiors 85, 131–142.

Venkateshwarlu, M., Chalapathi Rao, N.V., 2013. New palaeomagnetic and rock magnetic results on Mesoproterozoic kimberlites from the Eastern Dharwar craton, southern India: Towards constraining India's position in Rodinia. Precambr. Res. 224, 588–596.

Vermeesch, P., 2018. IsoplotR: a free and open toolbox for geochronology. Geosci. Front. 9, 1479–1493.

Veselovskiy, R.V., Bazhenov, M.L., Arzamastsev, A.A., 2016. Paleomagnetism of Devonian dykes in the northern Kola Peninsula and its bearing on the apparent polar wander path of Baltica in the Precambrian. Tectonophys 675, 91–102.

Wabo, H., De Kock, M.O., Beukes, N.J., Hegde, V.S., 2020. Palaeomagnetism of the uppermost carbonate units of the Purana basins in southern India: new demagnetization results from the Kaladgi and Bhima basins, Karnataka. Geol. Mag. 159, 269–278.

Wabo, H., Beukes, N.J., Patranabis-Deb, S., Saha, D., Belyanin, G., Kramers, J., 2022. Paleomagnetic and $^{40}Ar/^{39}Ar$ age constraints on the timing of deposition of deep-water carbonates of the Kurnool Group (Cuddapah basin) and correlation across Proterozoic Purana successions of Southern India. J. Asian Earth Sci. 223, 104984. https://doi.org/10.1016/j.jseaes.2021.104984.

Wadia, D.N., 1919. Geology of India for Students. MacMillan & Company, London, p. 398.

Warnock, A.C., Kodama, K.P., Zeitler, P.K., 2000. Using thermochronometry and low-temperature demagnetization to accurately date Precambrian paleomagnetic poles. J. Geophys. Res.: Solid Earth 105, 19435–19453.

Weil, A.B., Van der Voo, R., Mac Niocaill, C., Meert, J.G., 1998. The Proterozoic supercontinent Rodinia: paleomagnetically derived reconstructions for 1100 to 800 Ma. Earth Planet. Sci. Lett. 154, 13–24.

Wetherill, G.W., 1956. Discordant uranium-lead ages, I. Eos Trans. Am. Geophys. Union 37, 320–326.

Wingate, M.T., Pisarevsky, S.A., Evans, D.A., 2002. Rodinia connections between Australia and Laurentia: no SWEAT, no AUSWUS?. Terra Nova 14, 121–128.

Yadav, P., Sarma, D.S., Parashuramulu, V., 2020. Pb-Pb baddeleyite ages of mafic dykes from the Western Dharwar Craton, Southern India: a window into 2.21–2.18 Ga global mafic magmatism. J. Asian Earth Sci. 191, 104221. https://doi.org/10.1016/j.jseaes.2019.104221.

Yedekar, D.B., 1990. The central Indian collision suture. Geol. Surv. India Spec. Publ. 28, 1–43.

Yin, A., Dubey, C.S., Kelty, T.K., Webb, A.A.G., Harrison, T.M., Chou, C.Y., Célérier, J., 2010. Geologic correlation of the Himalayan orogen and Indian craton: Part 2. Structural geology, geochronology, and tectonic evolution of the Eastern Himalaya. Geol. Soc. America Bull. 122, 360–395.

Yoshida, M., Jacobs, J., Santosh, M., Rajesh, H.M., 2003. Role of Pan-African events in the Circum-East Antarctic orogen of East Gondwana: a critical overview. Geol. Soc. Lond. Spec. Publ. 206, 57–75.

Zhao, G., Cawood, P.A., Wilde, S.A., Sun, M., 2002. Review of global 2.1–1.8 Ga orogens: implications for a pre-Rodinia supercontinent. Earth-Sci. Rev. 59, 125–162.

Zhao, G., Sun, M., Wilde, S.A., Li, S., 2003. Assembly, accretion and breakup of the Paleo-Mesoproterozoic Columbia Supercontinent: records in the North China Craton. Gondwana Res. 6, 417–434.

Zhao, G., Sun, M., Wilde, S.A., Li, S., 2004. A paleo-mesoproterozoic supercontinent: assembly, growth and breakup. Earth-Sci. Rev. 67, 91–123.

Zhao, G., Li, S., Sun, M., Wilde, S.A., 2011. Assembly, accretion, and break-up of the Palaeo-Mesoproterozoic Columbia supercontinent: record in the North China Craton revisited. Int. Geol. Rev. 53, 1331–1356.

Zhao, J.H., Pandit, M.K., Wang, W., Xia, X.P., 2018b. Neoproterozoic tectonothermal evolution of NW India: Evidence from geochemistry and geochronology of granitoids. Lithos 316, 330–346.

Zhao, G., Wang, Y., Huang, B., Dong, Y., Li, S., Zhang, G., Yu, S., 2018a. Geological reconstructions of the East Asian blocks: from the breakup of Rodinia to the assembly of Pangea. Earth-Sci. Rev. 186, 262–286.

Zhao, H., Zhang, S., Ding, J., Chang, L., Ren, Q., Li, H., Yang, T., Wu, H., 2020. New geochronologic and paleomagnetic results from early Neoproterozoic mafic sills and late Mesoproterozoic to early Neoproterozoic successions in the eastern North China Craton, and implications for the reconstruction of Rodinia. Geol. Soc. America Bull. 132, 739–766.

Zhong, S., Zhang, N., Li, Z.X., Roberts, J.H., 2007. Supercontinent cycles, true polar wander, and very long-wavelength mantle convection. Earth Planet. Sci. Lett. 261, 551–564.

Zijderveld, J.D.A., 2013. AC demagnetization of rocks: analysis of results. In: Collinson, D.W., Creer, K.M., Runcorn, S.K. (Eds.), Methods in Palaeomagnetism. Elsevier, pp. 254–286.